Computational Study of Charge conducting Spacer molecules in Lead Chalcogenide Quantum dots

A Thesis

Presented to the Faculty of the Graduate School

of Cornell University

In Partial Fulfillment of the Requirements for the Degree of

Master of Science

by Santoshkalyan Chakravarthy Rayadhurgam

MAY 2015

ABSTRACT

Quantum dots (nanocrystals) have found applications in transistors, medical imaging,and solar cells, since they have band gaps that can be tuned into the far infrared region. This tuning is typically difficult to achieve with traditional semiconductor materials. The band gap tuning and self-assembly into a variety of large two-dimensional & three-dimensional superlattices makes them ideally suited for use in photovoltaic devices and other optoelectronic applications. Colloidal quantum dots of low band gap materials, like lead chalcogenide nanocrystals, have been the focus of considerable research efforts due to their potential ability for multiple exciton generation that theoretically may lead to efficiencies exceeding the Shockley-Queisser limit. However, quantum yield is greatly affected by the presence of capping ligands. The alkyl chain ligands presently used to prepare colloidal quantum dots are insulating in nature and, hence, impede charge transfer. Recent studies on ligand length have shown that charge transport decays as a function of the inter-quantum dot distance. In this study, we have introduced a new class of planar - charge conducting spacer molecules. We have used Molecular Dynamics simulations to understand the behavior of such spacer-capped lead chalcogenide quantum dots. We have determined force fields to describe the interaction between these planar spacers and the nanocrystals. We have investigated the behavior of aggregation of these planar molecules surrounding arrays of quantum dots. Specifically, we have calculated the energy preference of stacking these planar molecules on each other (aggregation) versus interaction of the spacers with the surface of the quantum dots. Our results for the radial distribution function of the spacer molecules and a study of their displacement indicate that these planar spacer molecules help avoid the sintering of quantum dots and reduce the distance between quantum dots to a significant extent compared to the previously used functionalized alkyl chain ligands.

DEDICATION AND ACKNOWLEDGEMENTS

This thesis is dedicated to my mother who passed away months before the completion of this effort.

I owe gratitude to my advisor Professor Paulette Clancy, who played a decisive role in my academic and professional development. Her advice and guidance expanded my interests in the field of Computational science. I will always be in her debt for the moral support and encouragement she gave me when my mother was diagnosed with terminal cancer. This thesis could not have been completed without her encouragement and direction.

Furthermore, I have to thank Professor Nandini Ananth, Professor David Bindel, Steve Thompson for their assistance, suggestions and accessibility for various issues that arose during this research effort. In addition, I want to thank Dr. Binit Lukose who introduced me to computational materials and provided valuable suggestions. I thank all the members of Clancy research group, especially Kristina, Brian, James, Jonathan and Tori for their valuable suggestions and help during my stay at Cornell.

I am grateful to my father who supported my study at Cornell amidst all the hurdles,as well as my family members : Lucky, Vindya, Vinay, Ram uncle for their enthusiastic support. Finally, I thank my friends Chaitanya, Sadashiv, Bikash, Deeksha and Atheendra for the moral support.

Biographical Sketch

Santoshkalyan Rayadhurgam earned his Bachelor of Engineering degree in Chemical Engineering from National Institute of Technology in India in 2010 , worked as a Process Engineer at Vedanta Resources and conducted research at Indian Institute of Science before joining the Department of Materials Science and Engineering at Cornell University in 2013. In May 2015, he will graduate with a Master of Science degree, with a focus on computational materials. Mr. Rayadhurgam has worked with Professor Paulette Clancy on Computational Materials research. He spent his summer at Cornell performing research in Professor Clancy's group and as a teaching assistant in the Department of Chemistry. Outside research, Santosh got involved in parallel computing, data science and electronic commerce projects, he held diverse roles : teaching assistant in the Cornell Graduate School of Business, teaching assistant in the Department of Chemistry, project manager at Cornell Data Science Club, computer assistant at Cornell Library. These experiences provided him with valuable experience and insight into graduate research, software development, and leadership. Upon graduation, Santosh will be working as a Software Developer with a technology firm in New York.

TABLE OF CONTENTS

List of Tables

Table **Page**

LIST OF FIGURES

FIGURE **Page**

CHAPTER 1

INTRODUCTION

1.1 Photovoltaic Materials

1.1.1 Introduction

The discovery of the photovoltaic effect by Becquerel in 1839 paved the way for solar cell development. Chapin, Fuller and Pearson developed the first solar cell by creating a silicon p-n junction, with enough efficiency for commercial applications in 1954 [25]. This device was termed the Bell Solar Battery. The era of satellites played an interesting early role in the development of solar cells when the Soviet Union launched Sputnik, a satellite powered completely by solar cells. Solar cells remained a technical novelty, limited to space applications until oil shortages became a reality and appropriate technology led their advance.

Photovoltaic cells require an extended sequence of successful photophysical processes in order to efficiently convert sunlight into electrical energy. The fundamental sequence is basically as follows: light absorption generates an electronically excited state. This excited state must either appear at, or migrate to, an interface, or heterojunction, where electron transfer can take place. Then the oxidized and reduced species (holes and electrons) must be able to migrate to opposite sides of the cell where they can be collected as electrical energy. A typical solar cell thus needs at least three key components: a light-absorber (dye), a hole-transport agent, and

an electron-transport agent. Sometimes one component is forced to fulfill multiple duties, as in a typical silicon cell, where silicon is the absorber which also serves as either a hole-transport (p-type) or electron-transport (n-type) agent with different doping. Many organic solar cells apply a similar approach, using light-absorbing dyes as charge-transport agents. Other approaches separate all three functions to be performed by different materials.

The core temperature of the sun is 20,000,000 K and the surface temperature is 6,000 K. At these high temperatures, the sun emits radiation in a manner that can be approximated as a black body. Figure 1.1 shows a black body spectrum at 5,670 K [27]. The extraterrestrial solar spectrum measured above earth‘s atmosphere is called the air mass zero (AM0) spectrum, and the solar spectrum measured on earth‘s surface at a latitude of 41 degrees is called the air mass 1.5 (AM1.5) spectrum. These standard spectra are used to quantify solar cell performance and are also shown in figure 1.1. The absorption and scattering losses in earth‘s atmosphere account for the difference in intensity and profile between the spectra.

Semiconductors used in p-n junction solar cells have a theoretical, limiting value of the efficiency known as the Shockley-Quiesser limit (or detailed balance limit) [20]. Fig. 1.1 shows the maximum theoretical efficiency of a single p-n junction solar cell. This calculation places a maximum solar conversion efficiency of around 33.7% at a band gap of 1.4 eV. The real gain in efficiency occurs if we can access above the Shockley-Quiesser limit.

Electron-hole pair multiplication occurs when more than one electron-hole pair is produced by absorption of one photon with an energy at least twice the semiconductor band gap. This process is referred to as 'impact ionization' in bulk semiconductors. It is observed in bulk silicon, Ge, PbSe, PbS and InSb.

Werner *et al.* [63] have showed that more than one electron-hole pair can be generated by one photon from the blue end of the solar spectrum. The ultraviolet photon excites a transition $e_1 - h_1$ at the first direct band gap in the silicon's band structure. Carrier multiplication occurs by optically induced Auger generation where the hot electron with excess energy undergoes inverse Auger relaxation towards the conduction band minimum near X. Energy, E, and momentum, K, are conserved by this transition, resulting in the production of two electron pairs. However, carrier multiplication in bulk semiconductors is not useful for solar photovoltaics as the required photon

(a)

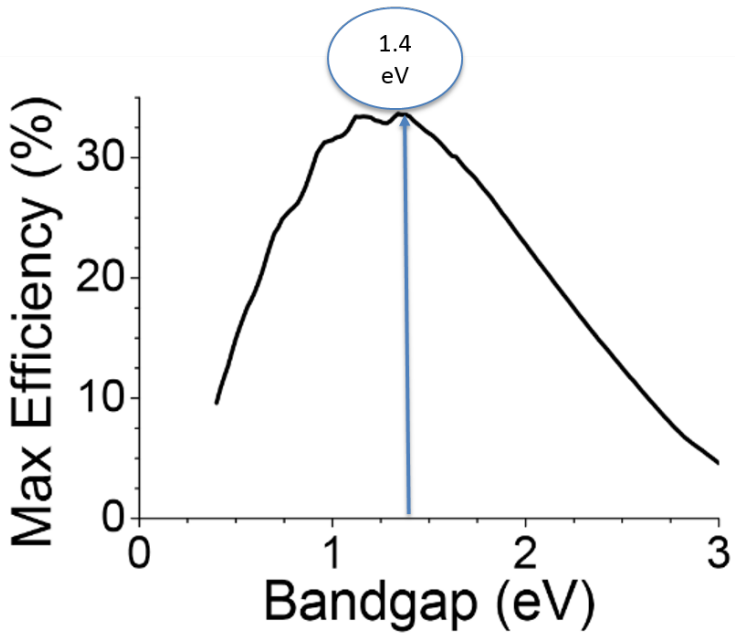

(b)

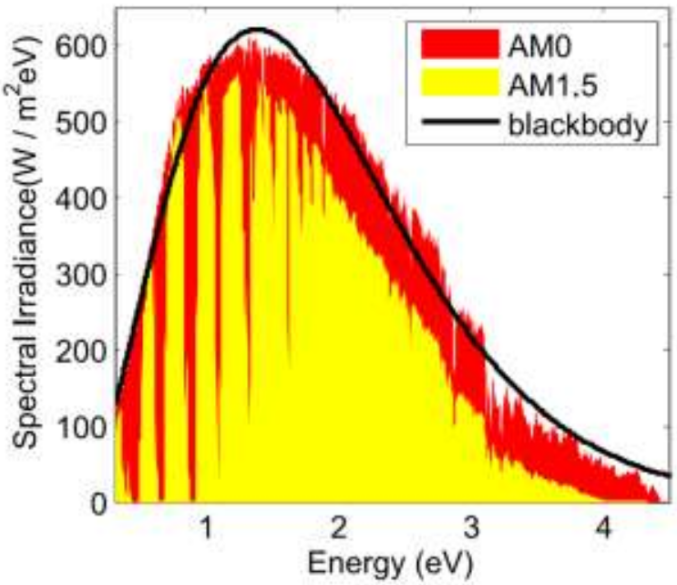

FIGURE 1.1. (a) Maximum Efficiency vs. Band Gap (b) Extra-terrestrial solar spectrum AM0, AM1.5 and black body spectrum at 5670 K

energy is outside the solar spectrum. No discussion on solar photovoltaics is complete without including a current version of the revised world-record solar cell power conversion efficiency chart, compiled by the National Renewable Energy Laboratory (NREL), shown in Figure 1.2.

(a)

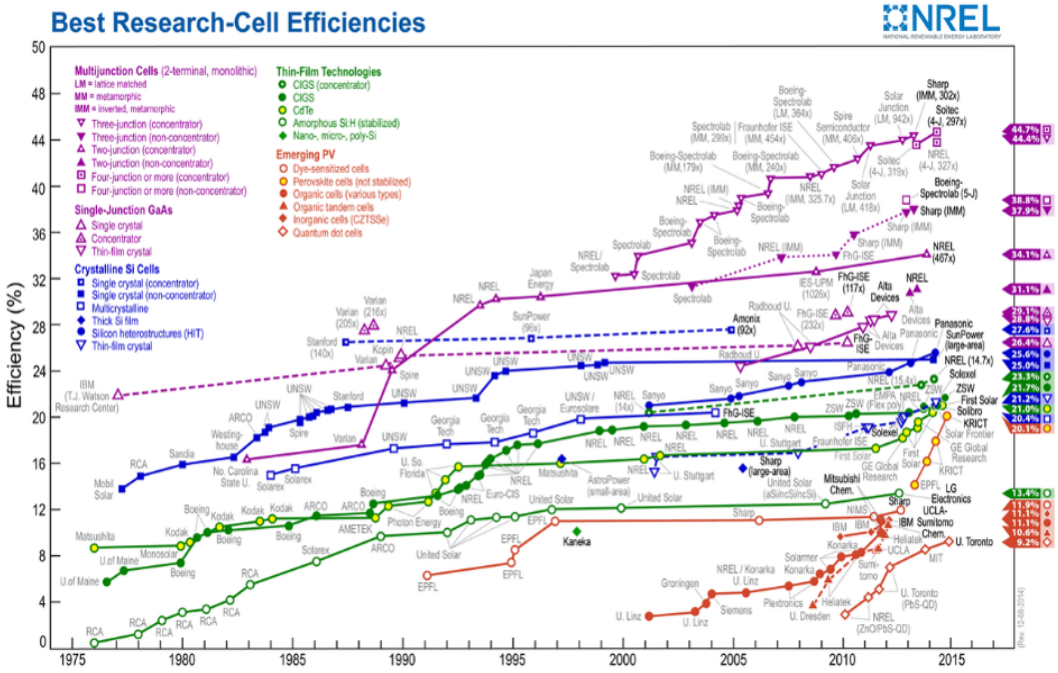

FIGURE 1.2. Solar power conversion efficiency records for major classes of solar cells. Courtesy of NREL.

1.1.2 Semiconductor nanocrystals (quantum dots)

Quantum dots are finite-sized semiconductors whose characteristic distances are measured on the nanoscale. Quantum dots are size-restricted such that the electron wave functions are confined within the volume. The 3-D confinement of charge carriers in a quantum dot transforms the continuous optical spectrum of bulk semiconductor into a size-tunable, atomic-like spectrum with a series of peaks associated with discrete electronic transitions. Each peak can be attributed to an exciton (an electron-hole pair) and other excitonic states in the quantum dot. The Bohr radius of the exciton is given by (1.1)

$$a_B = \frac{4\pi\epsilon_0\epsilon_\infty h^2}{m_0 e^2}\left(\frac{1}{m_e} + \frac{1}{m_h}\right) \tag{1.1}$$

where m_e and m_h are the effective electron and hole masses, respectively. e_∞ corresponds to the high-frequency relative dielectric constant of the medium. Effective masses are very small compared to electrons at rest, resulting in a larger Bohr radius.

In the early 1980s, papers in the Russian literature, for example by Ekinmov and Efros, gave the first experimental and theoretical description of 3D quantum confinement of semiconductor nanocrystals. Electron-hole pair multiplication in quantum dots is enhanced compared to bulk semiconductors due to quantum size effects, such as the relaxed momentum conservation, modified carrier cooling rates and enhanced Auger process. Auger effect is a physical phenomenon in which the filling of an inner-shell vacancy of an atom is accompanied by the emission of an electron from the same atom. The emission and absorption spectra corresponding to the band gap of quantum dot is governed by quantum confinement principles in an infinite square well potential. As the particle size (energy wall) decreases, there is an increase in band gap; see Fig. 1.3a. Figure 1.3b shows a high-energy photon absorbed at a high energy level in the quantum dot, which decays into two or more electron-hole pairs at the first confined energy level.

The three independently adjustable parameters in quantum dots are: (i) the electronic structure of the quantum dot by tailoring the quantum confinement of the wave function, (ii) inter-dot coupling, (iii) self-assembly of the quantum dots into ordered superstructures.

An understanding of the physico-chemical nature of the quantum dot surface is essential to the design of quantum dots for applications in opto-electronic devices. Further, the need for homogeneity within the ensemble of quantum dots makes it an important factor to study.

1.1.3 Lead chalcogenide nanocrystals

Lead chalcogenide (PbX, where X = S, Se, Te) nanocrystals are a class of nanostructured semiconductor materials that possess excellent photosensitivity in the near-infrared (NIR) region with a tunable energy band gap, ranging from 0.3 to 2.0 eV. These nanocrystals (NCs) have a large exciton Bohr radius (PbS: 18 nm, PbSe: 46 nm, PbTe: 150 nm, respectively). Such large Bohr radii

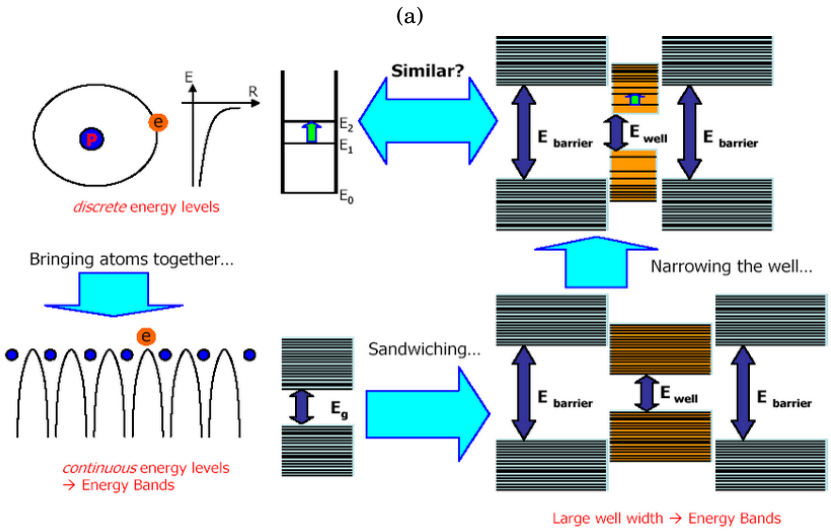

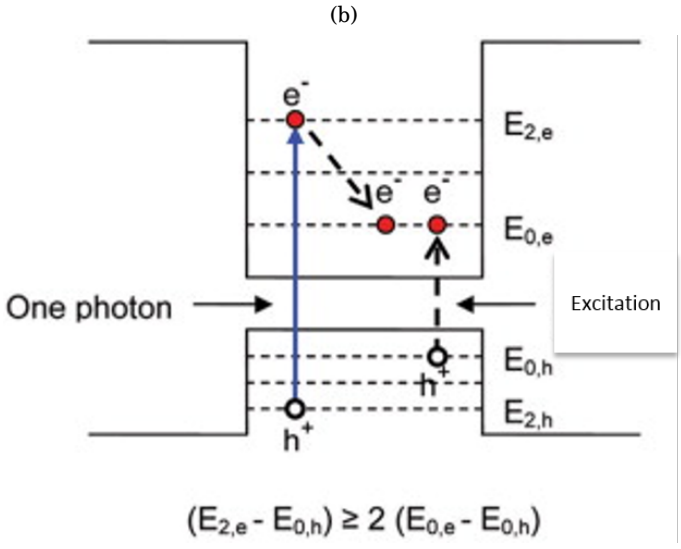

FIGURE 1.3. (a) Quantum confinement principle in an infinite square well potential (b) Multiple exciton generation in a quantum dot

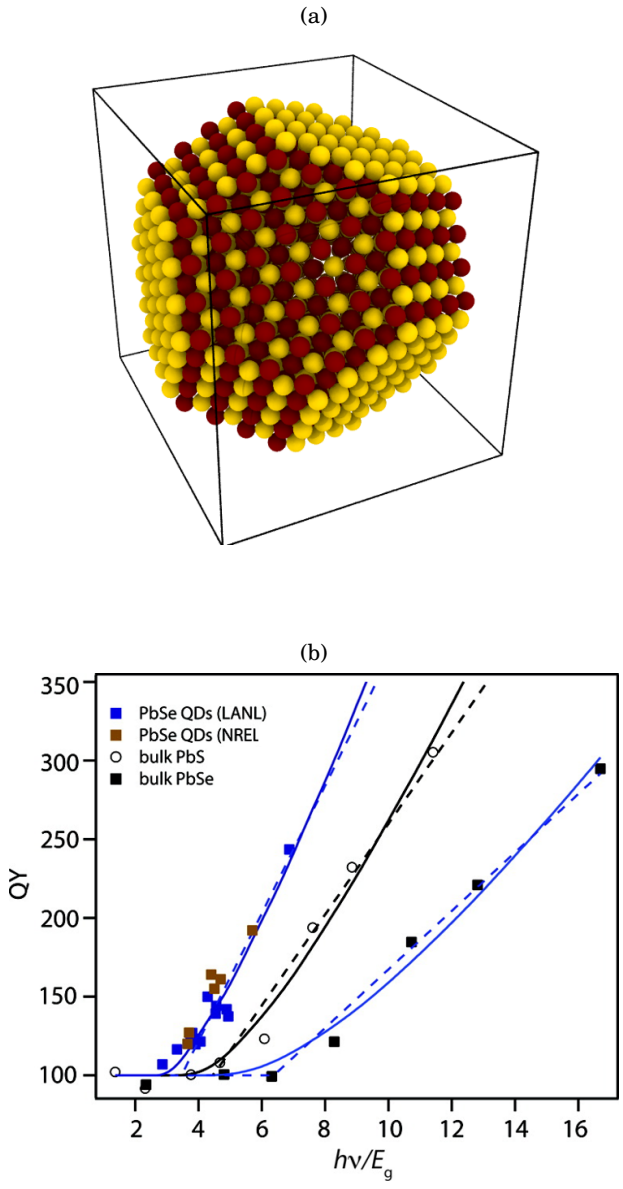

FIGURE 1.4. (a) Octahedral PbSe quantum dot (b) Quantum yield for PbSe quantum dots and bulk PbSe. Figure reproduced from [1]

and small masses for electrons and holes facilitate charge delocalization. And the high carrier mobilities and propensity for multiple exciton generation (MEG) in these materials makes them an excellent fit for applications in solar cells, photodetectors, thermoelectrics and lasers [7].

Figure 1.4b shows a plot of quantum yield for the lead chalcogenides for both quantum dots and bulk materials. It clearly indicates the increase in theoretical thermodynamic photovoltaic conversion efficiencies for quantum dot-based solar cells compared to bulk semiconductors.

For PbSe NCs, Quan *et al.* recently reported that a body-centered cubic (bcc) superlattice is the energetically most stable polymorph compared to face centered cubic (fcc) superlattice and body-centered tetragonal (bct) superlattice. They also showed that the stability sequence of PbSe NCs with a 4.7 nm diameter is consistent with the packing efficiency of PbSe NCs: bcc (17.2%), bct (16.0%) and fcc (15.2%) [61]

1.2 Colloidal synthesis of semiconductor nanocrystals

The properties of semiconductor nanocrystals have been investigated experimentally by studying the structures grown by high vacuum techniques such as molecular beam epitaxy (MBE) and metal-organic vapor phase epitaxy (MOVPE). Recent wet synthesis methods have enabled access to better control of size, shape and composition. Different emissions of wavelengths for quantum dots of different sizes are shown in Figure 1.5. These colorful fluorescent solutions exhibit the manifestation of quantum mechanics. By changing the size of the nanocrystals, we obtain a rainbow of colors, which clearly indicate that smaller particles emit higher energy photons as predicted by the Uncertainty Principle.

Colloidal semiconductor nanocrystals are composed of an inorganic core made up of a few hundred to a few thousand atoms surrounded by solubilizing ligands. Crystal sizes in the nanometer range result in a very high surface-to-volume ratio. Ligand stabilization is very essential in the formation of this high density of surface atoms in the co-ordination sphere.

Routes enabling controlled manipulation of nanocrystals into ordered states of matter lead to close-packed nanocrystals. Assembling these nanocrystals into solids gives rise to a new collective phenomena with interactions between proximal nanocrystals. This opens up possibilities of

making new devices with novel physical properties. Choi *et al.* studied the inter-nanocrystal coupling in lead chalcogenide nanocrystal assemblies [46]. Figure 1.5 shows the charge transfer rate as a function of inter-NC spacing.

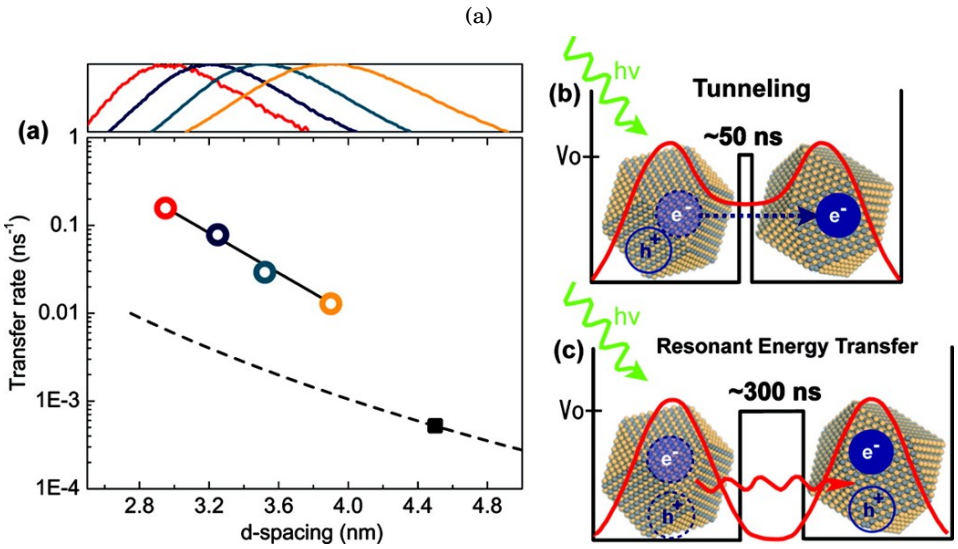

FIGURE 1.5. Plot of charge transfer rates with respect to inter-NC spacing. (b) Charge transfer rate calculated from exciton lifetimes. (c) Inter-nanocrystal distance measured with GISAXS [Figure reproduced from [46]]

1.2.1 Capping nanocrystals during colloidal synthesis

Classical studies on mono-dispersed colloids by La Mer and Dinegar [5] suggests that the production of nanocrystals requires a temporally discrete nucleation event followed by slower controlled growth on the existing nuclei. Figure 1.7 depicts the stages of nucleation and growth as suggested by the La Mer model. Murray *et al.* [52] carried out a hot-injection method in which chemical interactions between solvent, ligand and precursor molecules introduces synthetic degrees of freedom to obtain nanocrystals of varying shape, size and composition. Subsequent research efforts on the synthesis front have included the consideration of inverse micelle methods, gas phase reactions and supercritical fluid approaches. Nanocrystals have also been prepared in solid matrices, such as glass. However, in that case, control over NC size and shape is not as refined in comparison to solution-based-approaches. Most of the organically passivated core NCs

typically exhibit surface-related trap states which act as non-radiative de-excitation channels for charge carriers; hence reducing the quantum yield. There have been recent advances in resolving the insulating barrier caused by the capping ligands which block the electronic coupling between the nanocrystals, by modifying the coupling across the nanocrystal boundary using suitable surface treatments [10].

The number of atoms near the surface of quantum dots and the surface area of the quantum dot is large. This large surface area is essential for charge trapping. The as-prepared colloidal quantum dots are usually coated with long-chain organic ligands which passivate their surface and stabilize colloidal suspension. This can be seen in figure 1.6b.

Long-chain carboxylic acids, phosphonic acids (e.g., oleic acid) alkanethiols (e.g., dodecanethiol), alkyl phosphine oxides (e.g., trioctylphosphine) and alkylamines (e.g., hexadecylmine) have all been used as surfactants in the past. The synthesis of compound semiconductors such as lead chalcogenides is typically achieved by injecting a chalcogen precursor like trioctylphosphine into a heated solution containing the preheated Pb precursor (which is typically in the form of an oleate). After the initial nucleation, the NC particles grow in the reaction environment for a specified growth period, which is followed by a temperature quench. By adjusting synthesis parameters such as the growth time, growth temperature, and precursor concentration, the diameter of the resulting nanocrystals in the product can be tuned. Some of the critical parameters that control carrier transport include inter-dot distance, nanocrystal surface chemistry, the nature of the capping species, nanocrystal orientation, and the uniformity in size distribution (typically not better than about 10 per cent). Use of long alkyl chain ligands provides colloidal stabilization and passivates the nanocrystal surface. However, their presence also impedes inter-dot electronic coupling. It has been reported that the presence of long-chain ligands on the nanocrystal surface results in a surface-to-surface spacing of less than 2 nm [10]. Many studies of electronic coupling in colloidal nanocrystal arrays indicate that when nanocrystal cores are surrounded by insulating organic ligands these ligands help in terms of solubility and passivation of the NC surface. But these ligand ”shells” effectively localize the electron and hole wavefunction across the quantum dots [52]. Several chemical approaches have been suggested to replace long-chain ligands with shorter ones or ”linkers.”

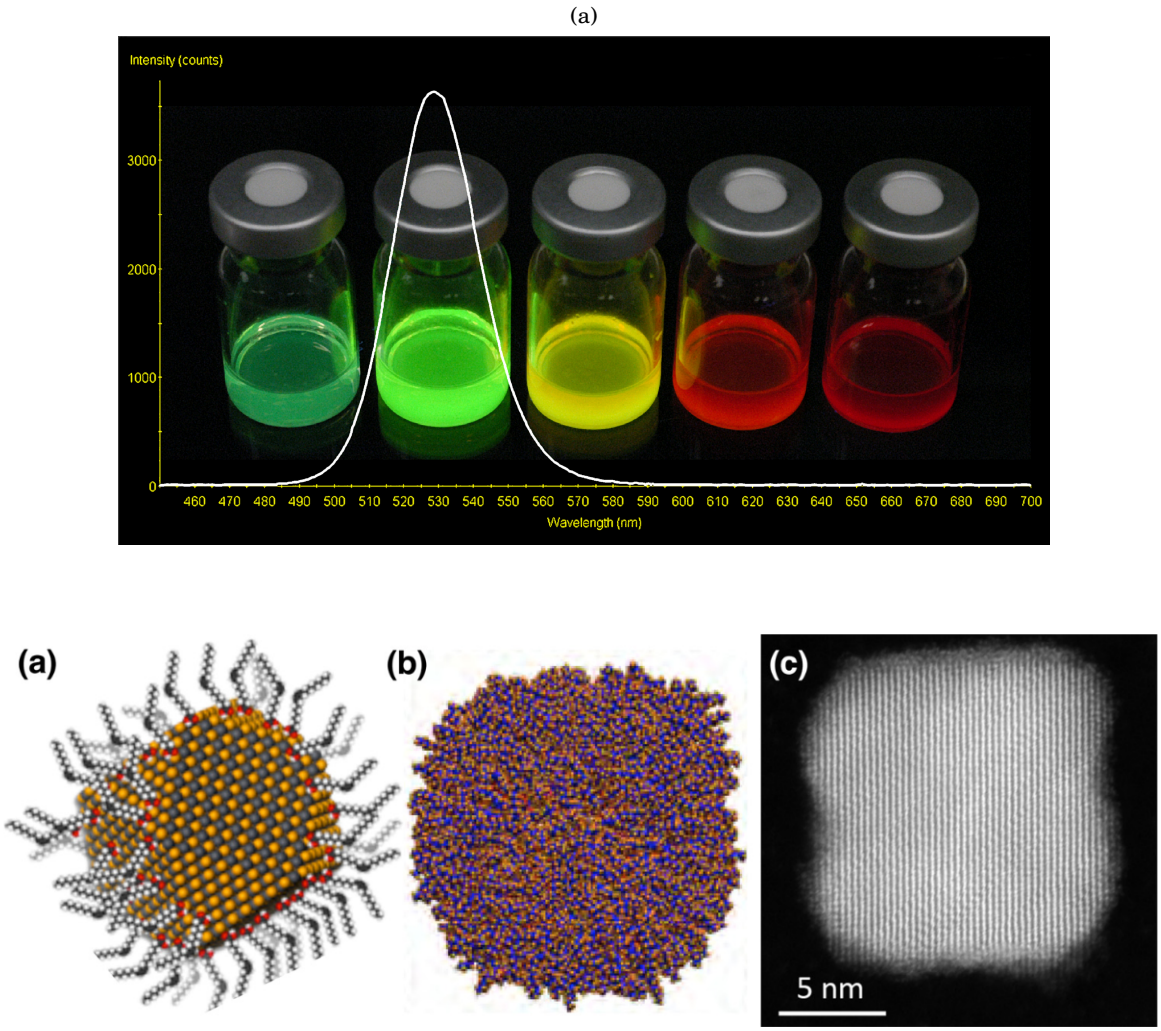

FIGURE 1.6. [Upper level image] (a) Photograph and representative photoluminescence spectrum of colloidal quantum dots excited by UV light. [Lower level images] (a) Basic schematic model of a single colloidal quantum dot showing some attached, stabilizing ligands. (b) Schematic of a NC fully covered in ligands. (c) TEM image showing faceting and crystal shape. [Figure reproduced from [10]]

1.3 Motivation for this study: Improving ligand design

To control and understand the inter-dot coupling, several attempts at re-designing the nature of the ligands have been made. One such method involves a ligand exchange procedure [52] that maximizes the removal of the original ligands by exposing the colloidal nanocrystals to an excess of a competitive ligand, resulting in either partial or complete exchange of the surface ligands. Guyot *et al.* [6] showed that exchanging phosphine oxide ligands on CdSe quantum dots with phenylenediamine results in an increase of three orders of magnitude in the conductivity. Murray and Talapin [3] reported that treating PbSe nanocrystal films with hydrazine removed the original oleic acid ligands and decreased inter-dot spacing from 1.1 to 0.8 nm, which increased the conductance by 10 orders of magnitude.

(a)

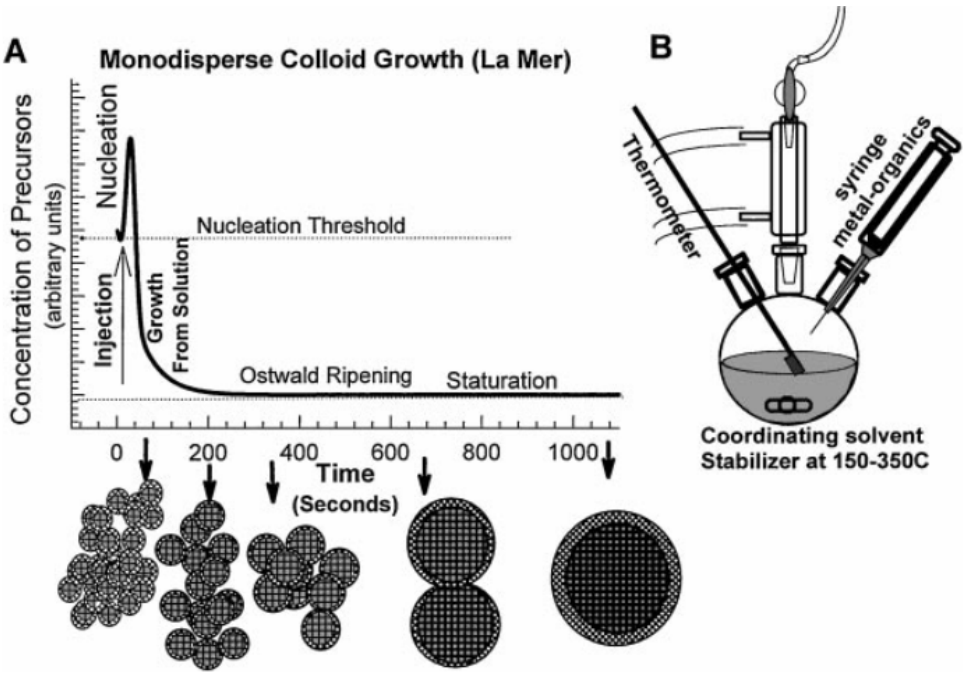

FIGURE 1.7. La Mer model: Stages of growth and nucleation

There is an inherent limitation of such solution-phase exchange of larger ligands with smaller ones; there is an ensuing decrease in colloidal stability often resulting in nanoparticle aggregation. However, to address this issue, ligand exchange can be performed, not in solution,

but on a superlattice. Choi *et al.* [46] illustrated the exponential relationship between inter-dot spacing and charge transfer rates. They concluded that exciton dissociation via tunneling of charge is the dominant pathway in the short inter-dot distance regime. Inter-dot charge transport cannot be improved further by using shorter or linking molecules. However, by employing capping molecules, such as conductive conjugated polymers and oligomers, Liu *et al.*[45] reported an improvement in charge transport in solar cells. Although significant progress has been made in designing better ligands for reducing the inter-dot distance, most of the work has involved using long-chain organic ligands which are insulating in nature. Thus, we saw an opportunity to test the feasibility of employing shorter ligands which are conducting, rather than insulating, and in this manner pave the way for more effective ligand designs that improve charge transport in self-assembled nanocrystal superlattices.

1.4 Phthalocyanine molecules as spacers

Phthalocyanines are a class of synthetic tetrapyrrolic compounds closely related to naturally occuring porphyrins [41]. Figure 1.8 shows the structure of phthalocyanine molecule with four isoindole units. Robertson [15] performed crystallographic studies of the structure of the ring system of metal-free phthalocyanine and indicated that at least two polymorphs exist for the phthalocyanine, a so-called x-form and a β form, shown in figure 1.9. Phthalocyanines have better photophysical and photochemical properties compared to the naturally occuring porphyrins [39]. Phthalocyanines have been extensively used as dyes and pigments. Most recently, phthalocyanines have found applications in ink-jet printing and photocopying devices. More than 70 elements can replace the hydrogen atoms of the central cavity [39].

The phthalocyanine macrocycle has sixteen ring sites available for possible substitution. These sixteen sites fall into two categories: peripheral sites (2,3,9,10,16,17,23,24) and non-peripheral sites (1,4,8,11,15,18,22,24), as shown in figure 1.10.

(a)

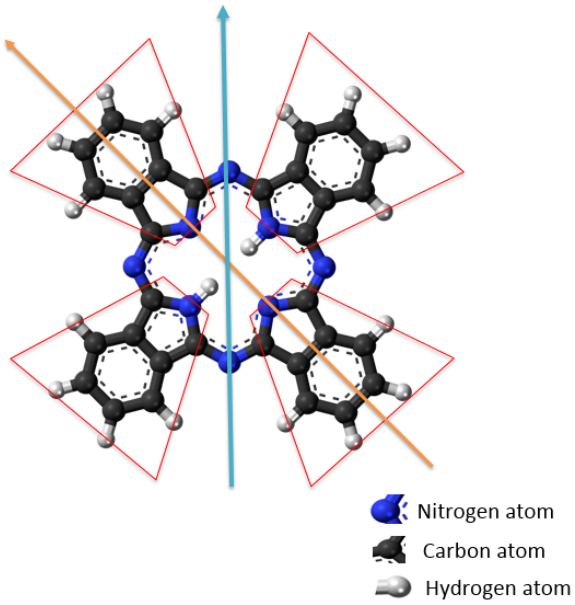

FIGURE 1.8. Structure of the metal-free phthalocyanine molecule

1.5 Prior Computational Efforts

Decades of research on studying ligand-capped nanocrystals has been limited to experimental investigations which typically lacked much insight into the role of the ligands and nanocrystals as you vary the process parameters such as temperature, aging, exposure to air, and choice of solvent. The nature of the ligands on the surface of the nanocrystal and the density of the ligands on different facets of the nanocrystal is still unclear. Such molecular-scale questions are very challenging to be described by experimental probes. This provides a significant motivation to employ molecular simulation approaches to supply this important information.

Molecular simulation studies by Leudkte *et al.* [49] and Schapotschnikow *et al.* [18] suggest that ligands play a very important role in the nanocrystal assembly process and passivate surface states. As such, it is incorrect to dubbed them merely as "spacers" between nanoparticles to prevent sintering. Leudkte *et al.* described the interactions of very small gold nanocrystals capped with thiol-terminated alkyl chains and showed that the core Au-Au interaction contributed to a

(a)

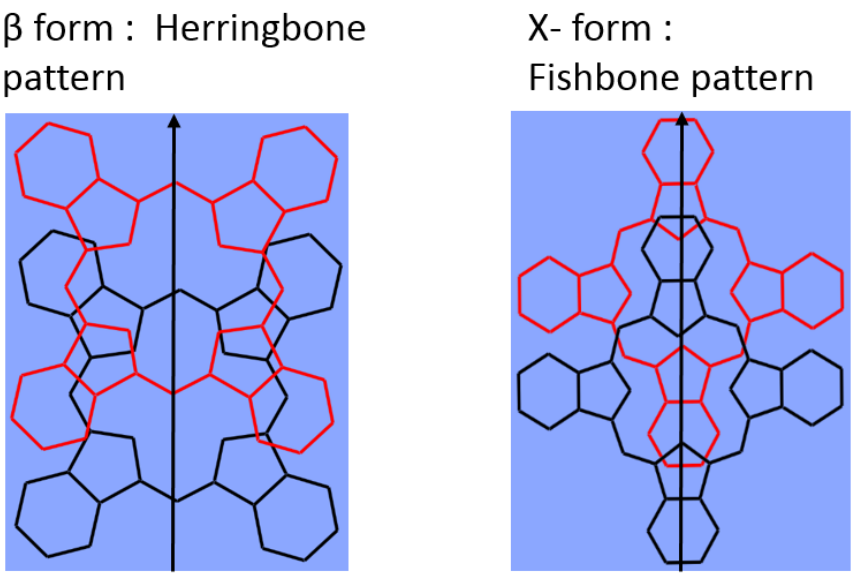

FIGURE 1.9. Crystallographic polymorphs of metal-free phthalocyanines

mere 1% of overall energy per particle in the system. The remainder of the energy is supplied by ligand-ligand interactions. They indicated a possible aggregation (”bundling”) of ligands at low temperatures as shown in figure 1.8 which has subsequently been shown to be an artefact caused by their choice of force field. They used a so-called ”United Atom” (UA) model, in which a group of atoms is represented as a "united atom" (or ”bead”) and treated using a mean field potential. In 1984, Jorgensen *et al.* [58] proposed the idea of UA models and showed agreeable results for liquid-like systems. However, a model suggested by Toxvaerd [62] concluded that the UA model suggested by Jorgensen *et al.* is unable to describe van der Waals interactions between carbon atoms and adjacent hydrogen atoms appropriately. In 1998, the TraPPE (transferable potentials for phase equilibria) force field was proposed by Siepmann *et al.* [21] which was successful in predicting phase equilibria of liquid mixtures. The issue of the erroneous Jorgenson model was revisited by Li *et al.* in 2010. They compared conformations of polyethylene chains using an explicit Dreiding model with the OPLS UA model. They suggested changes to the van der Waals interaction parameters to relieve the inflexibility of alkyl chains which led to an overly aggregated

(a)

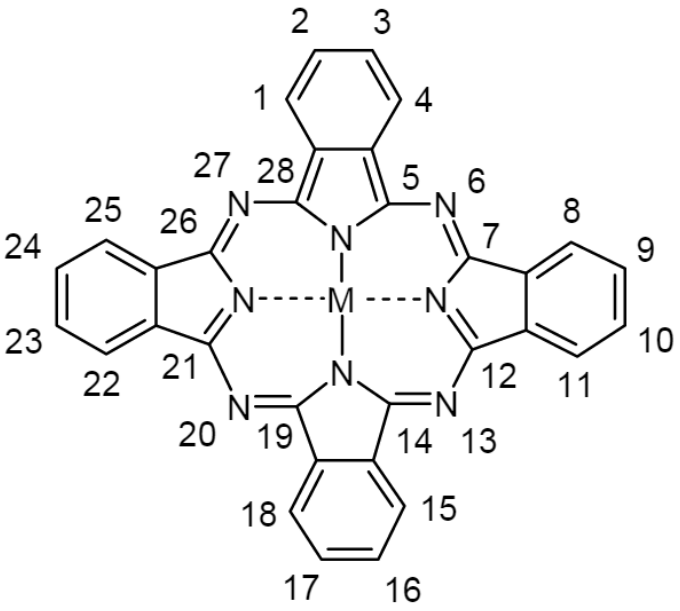

FIGURE 1.10. Peripheral and non-peripheral sites: numbering in a phthalocyanine-based molecule

conformation of the polymers. Further insight into this recurring issue was provided by Paul *et al.* [59] at IBM, whose intramolecular forces gave an improved representation of the UA interactions.

The specific choice of atom model, *via* appropriate descriptions of the intermolecular and intramolecular potentials, determine the conformations of molecules in a simulation. With the large number of models available in the literature with differing structural properties reported (as in the bundling phenomenon discussed above), it is clear that computational studies of NC-ligand system should be carried out with care. Rabani *et al.* used coarse-grained Lennard-Jones spheres as nanocrystals to study the interaction between nanocrystals in the presence of an implicit solvent. Yang *et al.* [64] studied the behavior of water molecules close to the surface of Au nanocrystals which are themselves capped with thiol ligands, as shown in figure 1.11. These studies indicate that ligands dictate the solvation shell formed by solvent molecules around ligand corona, thereby changing the strength of the interaction between the nanocrystals. Kaushik *et al.* [37] employed an explicit all-atom model to perform all-atom simulations of more realistically

(a)

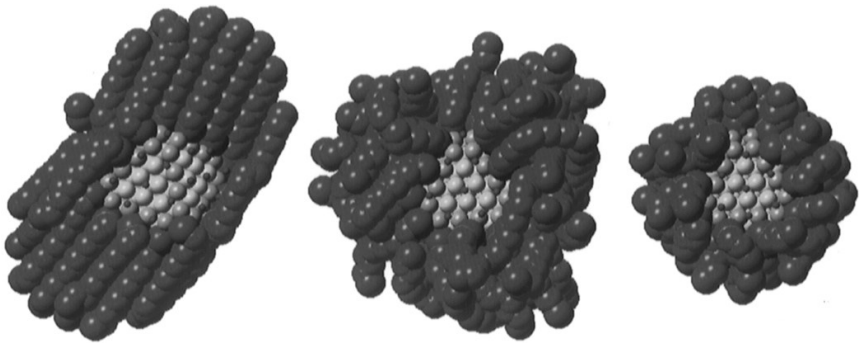

FIGURE 1.11. Equilibrium configurations of passivated Au isolated crystallites as described by Landman *et al.*. The structures at the left and middle correspond to low (200 K) and high-temperature (350 K) configurations for $Au_{140}C_{12}H_{25}S_{62}$ illustrating a bundling phenomenon at low temperatures which has since been largely discredited by subsequent work by Toxvaerd, Li, Paul and Kaushik. [Figure reproduced from [49]]

sized nanocrystals than had preiously been possible. In their work, alkyl chain ligand-capped nanocrystalline arrays of PbSe quantum dots were described using the MM3 potential of Allinger *et al.* for the ligand-ligand interactions and employing the Paul *et al.* model for the dihedrals to avoid the bundling issue.

In this thesis, we employ an explicit all-atom model to simulate the system of quantum dots with charge-conducting ligands. But, before we describe the details of our original research studies, the next chapter will first review some of the theory behind commonly used computational techniques used to study nanocrystals.

CHAPTER 2

MOLECULAR METHODS & PACKAGES

2.1 Molecular Methods

Computational models of the interactions between atoms can roughly be divided into two main classes of approaches, namely, larger-scale but less accurate semi-empirical representations and more accurate but more expensive *ab initio* quantum mechanical methods. As implied above, these methods differ in terms of accuracy, computational cost, and hence the length and time scales that they can be used to model. The most fundamental description of matter is one that invokes quantum mechanics. At the highest level of accuracy, this amounts to solving Schrodinger's equation for all of the subatomic particles in a system. Given the computational expense of this task, these *ab initio* techniques are limited, in practise, to small numbers of atoms (on the order of hundreds of atoms). There are both practical and philosophical reasons for performing simulations on simpler systems that do not entail a full solution of the quantum-mechanical equations. Figure 2.1 describes a hierarchy of simulation approaches that are tailored to treat the simulation of materials systems across different scales.

2.1.1 Molecular Dynamics

Molecular dynamics (MD) simulation is a technique by which the atomic trajectories of a system of N particles is generated by numerical integration of Newton‘s equation of motion, for a pre-

(a)

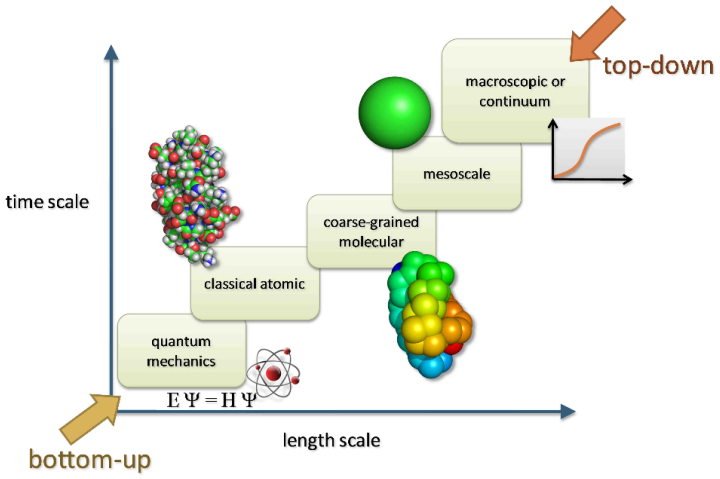

FIGURE 2.1. Multiscale Modeling: Hierarchy of simulation approaches that treat systems across different length- and time- scales

specified interatomic potential, with choices of initial condition, thermodynamic ensemble, and boundary conditions. MD was originally conceived in 1950s,and has evolved into a widely used theoretical tool that allows researchers in chemistry, physics and biology to model detailed microscopic dynamical behavior of many different types of systems, e.g., gases, liquids, and solids, as well as surfaces and clusters. MD is founded upon the basic principles of classical mechanics. It can provide a window into the microscopic dynamical behavior of the individual atoms that make up a given system. In addition to providing a microscopic dynamical picture, MD is also employed as a means of sampling from a chosen statistical mechanical ensemble and determining equilibrium properties such as structure, free energies along a reaction path, and average thermodynamic quantities (pressure, temperature, volume, etc.).

In contrast with the Metropolis Monte Carlo method, MD is a deterministic technique that simulates the time evolution of a molecular system and provides the actual trajectory of the system through phase space. The information generated from the simulation methods can, in principle, be used to characterize fully the thermodynamic state of the system. In MD, the evolution of the molecular system is studied as a series of snapshots taken at close time intervals (usually of the order of femtoseconds, in which 1 fs = $10^{-15}s$). Computational complexity increases

as the size of the system, and supercomputers or specialized attached processors (e.g., GPUs) may be needed to perform very large sized simulations and or simulations spanning long time periods. Based on the gradient of the potential energy function, **V**, the components F_i of the force **F** acting on an atom can be represented by equation (2.1). This force results in an acceleration, **a**, according to Newton's equations of motion (2.2).

$$F_i = -\nabla_i V \tag{2.1}$$

$$F_i = m_i a_i \tag{2.2}$$

$$-\frac{dV}{dr_i} = -m_i \frac{d^2 r_i}{dt^2} \tag{2.3}$$

A trajectory is calculated in a 6N - dimensional phase space (3N positions and 3N momenta). MD is a statistical mechanics method to obtain a set of configurations according to a statistical distribution function or statistical ensemble. For example, in a microcanonical ensemble, the Dirac function δ corresponding to a probability density in phase space, where the total energy is constant, selects only those states with a specific energy, E.

$$\delta(H(\Gamma) - E) \tag{2.4}$$

where, δ represents the Dirac function, Γ represents the set of positions and momenta and H(Γ) represents the Hamiltonian.

To use the force on each particle described in [2.1], the gradient of the potential energy function is required to be calculated [2.2]. Single atoms will be affected by the potential energy function of every atom in the system of bonded neighbors and non-bonded atoms.

In a canonical ensemble, the temperature, T, is constant and the probability density is the Boltzmann function,

$$exp\Big(-\frac{H(\Gamma)}{k_B T}\Big) \tag{2.5}$$

In MD, the Verlet algorithm is perhaps the most commonly used algorithm for time-integration. Verlet considers two third-order Taylor expansions for the determination of positions **r(t)**, one a step forward and one a step backward in time.

$$r(t+\Delta t) = (r(t) + v(t)\Delta t + \frac{a(t)\Delta t^2}{2} + \frac{b(t)\delta t^3}{6} + O(\Delta t^4) \tag{2.6}$$

$$r(t-\Delta t) = (r(t) - v(t)\Delta t + \frac{a(t)\Delta t^2}{2} - \frac{b(t)\delta t^3}{6} + O(\Delta t^4) \tag{2.7}$$

Adding 2.9 and 2.10, the first and third derivatives cancel out and we can express the next time step in terms of the previous position and current acceleration.

$$r(t+\Delta t) = 2r(t) - r(t-\Delta t) + a(t)\Delta t^2 + O(\Delta t^4) \tag{2.8}$$

The truncation error of this algorithm is on the order of Δt^4. With this version of the Verlet algorithm, it is not possible to generate the velocity directly. Additional velocities are required to compute the kinetic energy which is part of the conservation of total energy, which verifies that the MD simulation is correctly proceeding. Velocities can be computed from the positions, as represented in equation 2.12, but the error in this expression is of the order Δt^2 rather than Δt^4

$$v(t) = \frac{r(t+\Delta t) - r(t-\Delta t)}{2\Delta t} \tag{2.9}$$

There are variations of the Verlet algorithm, such as the leap-frog algorithm and predictor-corrector algorithm which seek to improve velocity estimations.

For a MD simulation, choosing a suitable potential (a function **V(R)** of the positions of the nuclei) is the most important input. The simplest way of representing **V** is to write it as a sum of bonded and non-bonded interactions.

$$V(R) = E_{bonded} + E_{non-bonded} \tag{2.10}$$

$$E_{non-bonded} = E_{van-der-Waals} + E_{electrostatic} \tag{2.11}$$

Non-bonded interactions are the summation of van der Waals and electrostatic interactions. Atoms with no net electrostatic charge still tend to attract each other at short distances as long as they do not get too close. The Lennard-Jones (LJ) potential is the most commonly used way to represent van der Waals interactions. Once the atoms are close enough to have overlapping electron clouds, they will repel each other with a repulsive force, as described in Figure 2.2a.

The Lennard-Jones (12-6) potential is given by the following equation, where σ is the distance corresponding to the zero-energy crossing point and ε is the minimum energy of the potential. The parameters σ and ε are chosen to fit the physical properties of the material. The LJ potential is strongly repulsive at shorter distances, passing through 0 at r = σ and increase steeply as r decreases. The first term containing $\frac{1}{r^{12}}$ dominates at short distances and models the repulsion between atoms when they are close to each other. The exponent 12 was chosen on a practical basis, as it is easy to compute. The physical origin of repulsion between atoms is related to the Pauli principle which states that when the electronic clouds surrounding the atoms starts to overlap, the energy of the system increases abruptly.

$$\Phi_{LJ}(r) = 4\varepsilon\left[\left(\frac{\sigma}{r}\right)^{12} - \left(\frac{\sigma}{r}\right)^{6}\right] \tag{2.12}$$

The LJ potential also has an attractive tail at large distance, r, and reaches a minimum at 1.122 σ. The second term in equation 2.12, $\frac{1}{r^6}$ constitutes the attractive part of the potential. This attraction originates from van der Waals dispersion forces (induced dipole-induced dipole interactions due to fluctuating dipoles). They are weak interactions, but they dominate the bonding character of closed-shell systems (rare gases like Ar or Kr).

In MD, the interaction potential could, in principle, have an infinite range. The number of atomic pairs separated by a distance r grows as r^2 and, for infinite range, it becomes impractical

to compute. As a consequence, a cut-off radius, R_c, is established that disregards any interactions between atoms that are separated by a distance larger than R_c.

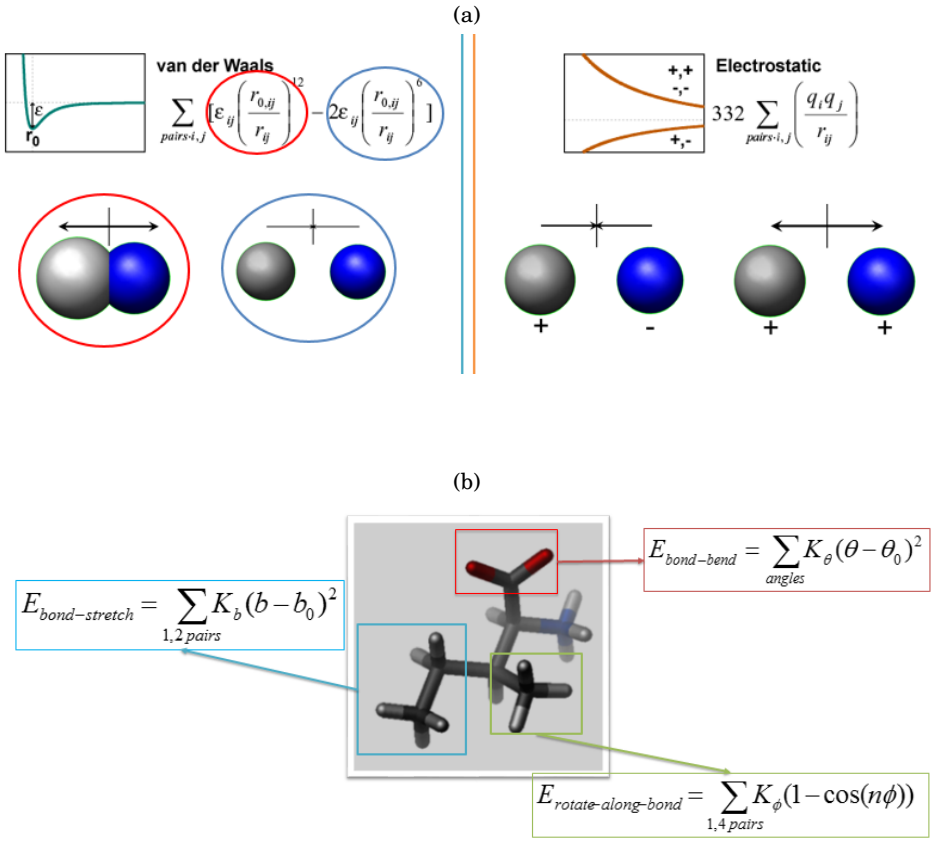

FIGURE 2.2. (a) Pictorial representation of non-bonded interactions: van der Waals interactions and electrostatic interactions (b) Pictorial representation of bonded interactions

In macroscopic systems, a tiny fraction of atoms are located near the boundaries. However, in MD simulations, which can handle system sizes up to on the order 10^6 atoms, the fraction of surface atoms can not be neglected. To solve this problem, Periodic Boundary Conditions (PBCs) are usually employed. In PBCs, the particles are enclosed in a box, which replicates to infinity by rigid translation in all three dimensions, filling space. The ”image” particles shadow the movements of the ”original” particle from the simulated box. When the particle leaves the simulation region, an image particle enters the region and *vice versa*, such that the number of particles being considered as part of the simulation box (or system) is always conserved.

Bonded interactions: In the bond stretch function, both the spring constant, K, and the ideal bond length are dependent on the nature of the atoms involved. Figure 2.2b depicts various bonded interactions. For bond angle functions, the spring constant and angle are dependent on the chemical nature of the atoms. The torsional potential is described by a dihedral angle and a coefficient of symmetry n = 1,2,3 around the middle bond.

$$E_{bonded} = E_{bond-stretch} + E_{angle-bend} + E_{rotate-along-bond} \tag{2.13}$$

2.1.2 *Ab initio* methods - Density Functional Theory

Quantum mechanics is the only known formulation of physics to deal with the electronic structure of molecules. Each electronic structure calculation is performed for a fixed nuclear configuration and therefore the positions of all atoms is specified as input. The time-independent Schrodinger equation describes the electronic structure for an N-particle system, where H is the Hamiltonian for a system of N electrons and M nuclei.

$$\mathbf{H}\Psi_i(\vec{x_1},\vec{x_2},\vec{x_3},...,\vec{x_M},\vec{R_1},\vec{R_1}...\vec{R_M}) = E_i\Psi_i(\vec{x_1},\vec{x_2},\vec{x_3},...,\vec{x_M},\vec{R_1},\vec{R_1}...\vec{R_M}) \tag{2.14}$$

By applying the Born-Oppenheimer approximation, nuclear and electronic motions are decoupled and treated separately. Each electronic structure calculation is performed for a fixed nuclear configuration. To find the energy states of electrons from the Hamiltonian, the Variational Principle is employed which states that the energy computed from a trial wavefunction gives an upper bound to the true ground-state energy, E_0. By iteratively adjusting the trial wave function to minimize E_0, an estimate of the true ground state energy can be obtained. Density functional theory (DFT) is one such technique to estimate this ground-state energy based on a spatially dependent electron density.

Computational costs are relatively low compared to traditional methods of estimating the electron wavefunction based Hartree-Fock theory. As such, DFT has been a successful approach for describing the ground-state properties of a wide variety of materials, from metals, to semicon-

ductors and insulators. The key variable in DFT is the particle density, $\rho(\vec{(}r))$, for a normalized Ψ and is given as

$$\psi(\vec{(}r)) = N \int ... \int \quad \text{mod } \Psi(\vec{x_1}, \vec{x_2} ... \vec{x_n})^2 dx_1 dx_2 ... dX_N \tag{2.15}$$

The interacting system is replaced by a non-interacting system as the real system uses two Hohenberg-Kohn theorems. E_{XC} is the exchange-correlation function that contains that which is not known about the self-interacting system. E_{XC} can be further split into E_X and E_C parts, which are the exchange and correlation parts, respectively. However, the exchange and correlation functions are only known fully for the free electron gas. However, there are widely used approximations which permit the accurate calculation of certain physical quantities. The most widely used approximation is the local-density approximation (LDA) where the functional depends only on the density at the coordinate where it is evaluated.

2.2 Molecular Simulation Packages

2.2.1 LAMMPS

LAMMPS is a classical Molecular Dynamics program which is an open-source code developed by Sandia National Laboratories. It is an acronym for Large-scale Atomic/ Molecular Massively Parallel Simulator. It is a C++ code capable of modeling atomic, biological, metallic, granular and polyatomic molecules by using a wide variety of force fields and boundary conditions. LAMMPS was originally designed for parallel applications but is commonly used in other configurations. It makes use of the Message Passing Interface (MPI) for parallel communication. The maximum number of atoms that can be modeled in a simulation depends on computational power. In most atomic systems, the time required for computing scales linearly with the number of atoms in the system. The same linear scaling does not hold for the number of processors and limitations occur when any code runs in parallel on a multiprocessor machine. The overhead associated with communicating between processors becomes important and, given enough processors, will eventually dominate the computational time [16].

A maximum of only 12 processors was used at any time in this work, so most of the simulation run time is spent on Molecular Dynamics rather than processor communication. LAMMPS uses spatial decomposition techniques to partition the simulation box into three-dimensional blocks which are divided among the processors. With MPI, processors communicate and store 'ghost' atoms, *i.e.*, information about other atoms bordering the processor's assigned region of space.

Popular MD codes like CHARMM and AMBER use atom-decomposition methods for parallelism. Like LAMMPS, other software suites such as NAMD and NWCHEM also use a spatial-decomposition approach. Although functions in LAMMPS are designed for easy modification, a good working working knowledge of C++ is necessary to make significant changes.

LAMMPS requires a list of molecular topology information such as mass and force field coefficients for each atom and the initial atomic coordinates as input, which can be entered at LAMMPS input script or can be generated by a user's code which is called when LAMMPS reads the input script. The simulation box is defined and filled with atoms. An example input file can be seen in figure 2.3. By defining an ensemble, and by keeping some properties constant, thermodynamic properties are controlled. Mechanical quantities like velocity and momentum can be explicitly assigned to a group or to individual atoms. When the system constraints are set, LAMMPS updates the system using a Verlet velocity integration (section 2.1.1.) for a pre-determined number of time steps.

The following is a representative input LAMMPS script to define the units, boundary, and different "styles" of the atoms.

```
units           real
atom_style      molecular
pair_style      lj/cut 20.0
bond_style      harmonic
angle_style     harmonic
dihedral_style  opls
boundary      p p p
read_data       data.start
```

LAMMPS performs an energy minimization of the system by adjusting the atomic co-ordinates iteratively. The minimization procedure stops if any of the following criteria are not met: the change in energy between the outer interactions is less than a pre-set stopping tolerance of the energy; the length of the global force vector is less than the stopping tolerance for force; the number of outer iterations or time steps exceeds the maximum iterations of the minimizer, and if the number of total force evaluations exceeds the maximum number of force/energy evaluations.

2.2.2 Visual Molecular Dynamics- VMD

VMD is designed to visualize molecular and biological systems. It is an open-source code developed in 1996 by *The Theoretical Biophysics Group* at the University of Illinois in Urbana-Champaign [57]. It provides an excellent graphical interface and a command prompt. It allows users to run their own Python and Tcl scripts. VMD provides a variety of color schemes and visualization styles.

A LAMMPS dump file provides the co-ordinates for all atoms of the simulation over a series of time steps in a properly-formatted text file, which is taken as an input to VMD. VMD facilitates a way of animating this abstract collection of data. To visualize an atom, VMD assigns a radius from the coordinate and fills the volume inside this radius with a solid color. VMD offers a wide choice of rendering methods, such as VDW (solid van der Waals spheres for atoms, no bonds), CPK - which is a space-filling model (scaled VDW sphere with cylinders for bonds) and a line-based representation. A screen shot depicting the VMD user interface can be seen in Figure 2.3.

If the system exhibited ant unusual packing of molecules, or atoms jumping away at high speed, or loss of atoms and any other unexpected phenomena, VMD was useful for visualizing these unusual and unwanted events allowing them to be traced back to errors in the input script.

2.2.3 PACKMOL

PACKMOL is a package for building initial configurations for Molecular Dynamics simulations. It was developed by Martinez *et al.* [51] in 2008. Obtaining a molecular arrangement where the simulations are not disrupted by van der Waals repulsive interactions is quite a challenging problem. PACKMOL was originally developed to pack millions of atoms, associated with different

molecules, optimally within a variety of three-dimensional regions of space. The input file is simple to make and supports XYZ, PDB, TINKER and other co-ordinate files. An example input script can be seen in following code block.

```
structure phthalocyanine_opt.xyz
  tolerance 3.5
  number 7000
  inside cube 0.0 0.0 0.0 300
end structure
output NCstructPBC.xyz
```

The keyword **structure** takes the input file and sets a tolerance distance using **tolerance** and fills up the cube with number of molecules specified by **number**. In this thesis, PACKMOL was used to generate the initial configurations of systems packed with ligand molecules in the presence of nanocrystals to a size of 140,000 atoms.

2.2.4 Gaussian

Gaussian is the most popular computational quantum chemistry software. It was initially released by John Pople *et al.* [48] at Carnegie Mellon University as Gaussian 70. It is a licensed software; the latest version is Gaussian 09, which is capable of predicting the properties of atoms, molecules and reactive systems like molecular energies, structures, vibrational frequencies, electron densities by utilizing *ab initio*, DFT, semi-empirical, molecular mechanics and other hybrid methods.

In this thesis, Gaussian 09 was used to perform geometry optimization and binding energy calculations. We have used the Minnesota functional, M06, developed by Donald Truhlar *et al.* at the University of Minnesota, which are a group of approximated exchange-correlations energy functionals in DFT. These functions are based on meta-GGA (generalized gradient approximation) and are popularly used functionals for solid-state physics and quantum chemistry calculations. The following code block shows a typical input code for a ground-state geometry optimization:

```
 #N B3LYP/6-31G(d) Opt Freq Test temperature =195
```

The keyword **Opt** performs the geometry optimization. Geometry optimization can be performed on internal co-ordinates and Cartesian coordinates. The level of theory chosen in this example is the **B3LYP** DFT method. The basis set is **6-31G(d)** adequate for first and second row elements.

In this thesis, we employ a dispersion-corrected DFT functional B3LYP-D3 which denotes a calculation employing the usual B3LYP functional plus a D3 dispersion correction energy term. The dispersion correction energy term D3 is a relatively simply function of interatomic distances and contain adjustable parameters that are fitted to conformational and interaction energies. Dispersion corrections lead to significant improvements in accuracy and the computational cost associated with dispersion corrections are negligible. We also employ the M06 suite of hybrid density functionals for both transition metals and non-metals.[66]

2.2.5 Molden

Molden is a pre- and post-processing software package for computational chemistry program data, developed by Schaftenaar *et al.* [42]. It has a powerful Z-matrix editor and reads the output from many *ab initio* packages like Gaussian, GAMESS and also supports xyz files. Molden also provides the tools to measure distance, angles and dihedrals between atoms. In this thesis, Molden was used as both a pre-processing tool to construct molecules, and as a post-processing tool to measure distances and angles between molecules.

2.2.6 OVITO

OVITO is an acronym for an Open Visualization Tool. It is a freely available visualization and data analysis code for atomistic data sets as output by large-scale Molecular Dynamics/statics and Monte Carlo simulations. It was developed by Alexander Stukowski [22]. OVITO is written in object-oriented C++, controllable *via* Python scripts.

CHAPTER 3

THESIS WORK

3.1 Organization of this Thesis

This thesis addresses an open question regarding the self-assembly of colloidal nanocrystal (NC) superlattices using suitable choices of solubilizing ligands.

In the first chapter, we have briefly introduced background information concerning solar cells, photovoltaic materials, and focused on quantum dots and their properties as a potentially useful photovoltaic solar cell material. A schematic of a typical nanocrystal in the size range that is of interest here (circa 3.0 - 7.0 nm) is provided for reference in Figure 3.1. We have discussed the theory behind the physics of the electronic structure of quantum dots (QDs) and described the novel electronic properties exhibited by quantum dots. Chapter 1 also provided a brief experimental background in the field of colloidal quantum dots, followed by a summary of previous computational modeling work on NCs.

The second chapter introduced the computational techniques that will be employed in this thesis, especially Molecular Dynamics (MD) and Density Functional Theory (DFT) which we used *via* existing software packages such as LAMMPS [16], GAUSSIAN [48] and tools such as VMD [57], MOLDEN [42], PACKMOL [51] and OVITO [22], all of which were used in this thesis.

This third chapter describes original research results regarding the study of phthalocyanine molecules as potential "spacers" in QDs. The central hypothesis of this thesis is that phthalo-

cyanine molecules, given their one atom-thick charge-conducting nature, would be a potentially better "spacer" for colloidal chalcogenide quantum dots than traditionally used spacers, which do not conduct electric charge and which are historically longer in length. Thus, the potential exists for this system of spacers to allow the NCs to pack together more closely and for the spacers to contribute constructively to improve charge transport. No experimental measurements of such a system have yet been carried out. Thus, these calculations could act as an important feasibility study in the consideration of a completely non-traditional approach to retaining NC quantum confinement while allowing the NCs to approach as closely as possible to maximize charge transport. The first task in this regard involves using *ab initio* calculations to determine the binding energies of phthalocyanine molecules to serve as a reference database to which Lennard-Jones parameters are fitted in order to create suitable force fields to describe both the phthalocyanine molecules and the NCs and their interaction. Once suitable models have been established, we present a series of increasingly complex simulations in which first one QD, then two QDs in close proximity, and then a superlattice array of QDs are placed in a box of phthalocyanine molecules. Critically, this study also examines the preference of phthalocyanine molecules to adsorb on specific NC facets in all of these test cases.

The fourth chapter in this thesis provides the conclusions of this study and offers a brief discussion about some of the future directions that can be taken to address still remaining grand challenges in nanocrystal superlattice formation for quantum dot solar cells.

3.2 Configuration of the system

This thesis is concerned with representing the properties of a nanocrystalline array of lead chalcogenide quantum dots (NCs) surrounded by phthalocyanine ligands. As discussed in Chapter 1, section 1.1.3, PbSe NCs prefer to adopt a body-centered cubic (BCC) superlattice as the most energetically favorable polymorph [61]. We consider each NC as having a BCC lattice structure made up of Pb and Se atoms. As mentioned above, our first task will be to determine an interatomic force model that adequately represents the interactions between Pb and Se atoms in the NC, as well as determining a suitable force field for phthalocyanine - phthalocyanine

interactions as well as phthalocyanine - nanocrystal interactions.

Experimentally, the size and shape of the NC is governed by temperature and by the concentration of the precursors used in the synthesis technique. Nanocrystals with diameter less than 3 nm are more or less octahedral in shape [37]. NCs with diameters in the range of 4-7 nm are of particular interest experimentally; they adopt a more cube-octahedral shape, exhibiting both {100} and {111} facets [54]. At diameters above this range, the NCs are typically cubic in shape.

In this study, we have considered NCs with a 4 nm diameter which, thus, display both {100} and {111} facets on their outer surface, as shown in Figure 3.1. The {100} facets can display either Pb-terminated or Se-terminated faces. It has yet to be seen, and will be explored in this thesis, if phthalocyanine molecules show a greater preference for adsorbing onto Pb atoms or Se atoms which, in turn, could alter the extent to which they adsorb on {111} versus {100} facets. This could then affect the relative orientation (and hence symmetry) of the NCs in the forming superlattice and perhaps alter the charge transport of the array.

The organic spacers chosen for this study are phthalocyanines, discussed in section 1.3.1. Phthalocyanine, $C_{32}H_{18}N_8$, is composed of 32 carbon atoms,18 Hydrogen atoms and 8 Nitrogen atoms, as shown in Figure 3.1b. The potential models and associated parameters for all the interactions between the ligands are described in the next section. The phthalocyanine spacer was created using the Molden software package [42]; discussed in section 2.2.5. An energy minimization of a tentative structure for the phthalocyanine molecule was performed using a standard minimization algorithm - the Polak-Ribiere version of a conjugate gradient algorithm, which is part of Sandia's LAMMPS software package [16]. At each iteration, the force gradient is combined with information from the previous iteration to compute a new search direction conjugate to the previous search direction.The Polak-Ribiere variant is thought to be the most effective conjugate gradient method choice for most problems in energy minimization [16].

3.3 Intermolecular Potential Models

In the Molecular Dynamics technique, the choice of inter- and intra- molecular potential model is a critically important determinant in the trajectory of atoms and molecules in the system. As

(a)

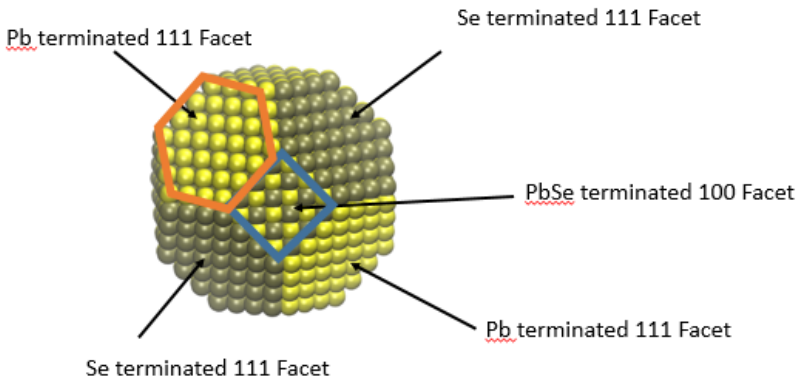

FIGURE 3.1. (a) Figure depicting different facets of a truncated PbSe nanocrystal with {111} Pb-rich, {111} Se-rich and {100} Pb-Se alternating facets

discussed in section 1.4, there are very few studies employing explicit all-atom simulations of quantum dots due to the large size of the systems for any realistic NC diameter and the associated computational effort that this implies. As a rare exception, Kaushik *et al.* [37] performed explicit all-atom simulations of FCC PbSe nanocrystal with chain ligands and showed the importance of using explicit all-atom model to provide reference data against which to judge the accuracy of coarse-graining the systems to reduce the computational effort of property determination.

In the calculations which follow, we employed the commonly used semi-empirical all-atom explicit Optimized Potentials for Liquid Simulations (OPLS-AA) potential, developed by Jorgensen *et al.* [58] to model all the phthalocyanine - phthalocyanine interactions. The OPLS-AA potential is an explicit all-atom force field representation in the same vein as force fields such as MM3, Dreiding, CHARMM, *etc.* [19, 38, 55].

The OPLS-AA potential incorporates bond stretching, angle bending and torsional energies, as well as the van der Waals interaction energies. One of the distinctive features of OPLS parameters is that they have been optimized to fit experimental properties of liquids, especially the liquid density, heat of evaporation,*etc.*

The functional form of the OPLS - AA force field is given in equations 3.1 - 3.5, as explained

more fully in section 2.1.1,

$$E_{r^N} = E_{bonds} + E_{angles} + E_{dihedrals} + E_{nonbonded} \tag{3.1}$$

$$E_{bond} = \sum_{bonds} K_r (r - r_0)^2 \tag{3.2}$$

where summing over bonds represents the energy between covalently bonded atoms. This harmonic (ideal spring constant K_r) force is a good approximation near the equilibrium bond length, but becomes increasingly poor as atoms separate.

$$E_{angle} = \sum_{angles} K_\Theta (\Theta - \Theta_0)^2 \tag{3.3}$$

where summing over angles, Θ, represents the energy due to the geometry of electron orbitals involved in covalent bonding.

$$E_\Phi = \frac{V_1}{2}[1 + cos(\Phi + f1)] + \frac{V_2}{2}[1 - cos(2\Phi + f2)] + \frac{V_3}{2}[1 + cos(3\Phi + f3)] \tag{3.4}$$

where summing over torsions, Φ, represents the energy for twisting a bond due to bond order, $f1$, (e.g., double bonds) and neighboring bonds, $f2$, or lone pairs of electrons, $f3$.

$$E_{nonbonded} = \sum_{i>j} \left(\frac{A_{ij}}{r^{12}} - \frac{C_{ij}}{r^6} + \frac{q_i q_j e^2}{4\pi\varepsilon_0 r_{ij}} \right) \tag{3.5}$$

Equation 3.5 employs standard combining rules for the unlike interactions for parameters A and C. $A_{ij} = A_{ii}{A_{jj}}^{1/2} and C_{ij} = C_{ii}{C_{jj}}^{1/2}$. Intermolecular non-bonded interactions are counted for atoms which are three or more bonds apart. The van der Waals potential takes the form of the Lennard-Jones potential described in section 2.1.1. The values of k_r, K_Θ, A , C are taken, without change, to be those given in the original OPLS-AA paper by Jorgensen *et al.* [58].

Simulating explicit all-atom models using the OPLS force field is computationally expensive. A system of 60,000 atoms simulated even for a short time, *e.g.,* for 100 ps, can take almost 24

hours to complete when run on a single processor of a Dell 410 with a 2.93 GHz Xeon core. Given the computational expense of all-atom simulations, the simulations reported in this thesis were limited to consideration of three test cases: (1) phthalocyanine molecules in the absence of a NC as a baseline study. (2) a single isolated 4 nm diameter NC of PbSe surrounded by phthalocyanine molecules; (3) a pair of 4 nm diameter PbSe NCs in close proximity, surrounded by phthalocyanine molecules; and (4) a BCC superlattice array of PbSe NC surrounded by, and interspersed with, phthalocyanine molecules. In all cases, the phthalocyanine molecules (in vapor and liquid phases) are not attached or tethered (covalently bound) to the NC surface.

3.4 Simulation methodology

The Molecular Dynamics simulations in this thesis were performed with a standard velocity-Verlet integrator, discussed in section 2.1.1., which is part of the LAMMPS package [16]. As discussed in the previous section, the optimized structures of the above mentioned systems were obtained from an energy minimization of initial guesses at their structures using the Polar-Ribiere implementation of a conjugate gradient algorithm. This thesis work considered the interactions among all the atoms composing the nanocrystal. We treated the NCs either as fixed (all the atoms in the NC are frozen to their initial positions by zeroing their force) or as a rigid body (where all coordinates, velocities, and orientations of a group of atoms in the NC are updated so that the body moves and rotates as a single entity), as the situation required. In the ligand-capped nanocrystal system studied by Kaushik *et al.*, the long oleic atoms were covalently attached to the NC surface at one end, and hence they studied nanocrystal-ligand interactions by approximating the core of the nanocrystal as a hollow shell. In this thesis, since the spacers are not bound to the surface of the nanocrystal, the spacers are initially placed close to (3.5 angstroms away from) the nanocrystal, and hence within the range of the NC's intermolecular forces. This allowed us to observe the interaction between phthalocyanine molecules and the NC's surface. Unlike Kaushik *et al.*,we need to consider not only the atoms on the surface of the NC but also those in the interior of the NC, to a distance of approximately 11.5 angstroms inside the surface. As discussed earlier, the 4 nm diameter truncated BCC octahedral shape of the

nanocrystal was considered as the structural model for the superlattice; see Figure 3.1. Modeling the interactions of NC with phthalocyanine molecules will be described in a later section. The preferential adsorption sites on the NC surface will also be studied in subsequent sections.

3.4.1 Methodology: Force Field Validation

The initial task of this study was performed to validate the force fields for the components of the system, and to optimize Lennard-Jones parameters for C-C,C-H,C-N,H-H,Pb-Pb,and Se-Se interactions.

Firstly, we performed a geometry optimization of AA stacked phthalocyanine molecules; see Figure 3.2a for a description of AA stacking. As discussed in section 2.2.4, we employed the dispersion-corrected B3LYP-D3 functional for geometry optimization of phthalocyanine using the **Gaussian09** package. A pair of phthalocyanine molecules in an AA stacking arrangement were moved apart in steps of 0.1 angstrom, allowing the interaction energy to be studied as a function of the distance of separation between the test pair of phthalocyanine molecules.See figure 3.2.,3.8.

Using the **LAMMPS** suite of programs, we optimized the LJ parameters in the OPLS-AA force field [58] by fitting the interaction energy as a function of distance between two phthalocyanine molecules against the *ab initio* data.see figure 3.8.

As a next step to optimize the LJ parameters of phthalocyanine further, we calculated the interaction energy between a pair of phthalocyanine molecules as a function of shifting one phthalocyanine molecule laterally across the surface of the other molecule, starting from a fully eclipsed (AA) position and ending at a fully staggered configuration; see Figure 3.2b. Using the *ab initio* data we had produced, we again adjusted the LJ parameters to optimize the fit to the *ab initio* data, in a manner similar to the previous step.

In the third fitting step, we optimized the LJ parameters of Pb and Se by fitting the interaction energy curve between one PbSe NC and one phthalocyanine molecule; see Figure 3.3. We first performed a geometry optimization of the system using an *ab initio* DFT study. For that study, we employed both the dispersion-corrected B3LYP-D3 functional for phthalocyanine and the Minnesota functional M06 (which is the most popular functional used for transition metals) for

the Pb and Se atoms using the **Gaussian09** package.

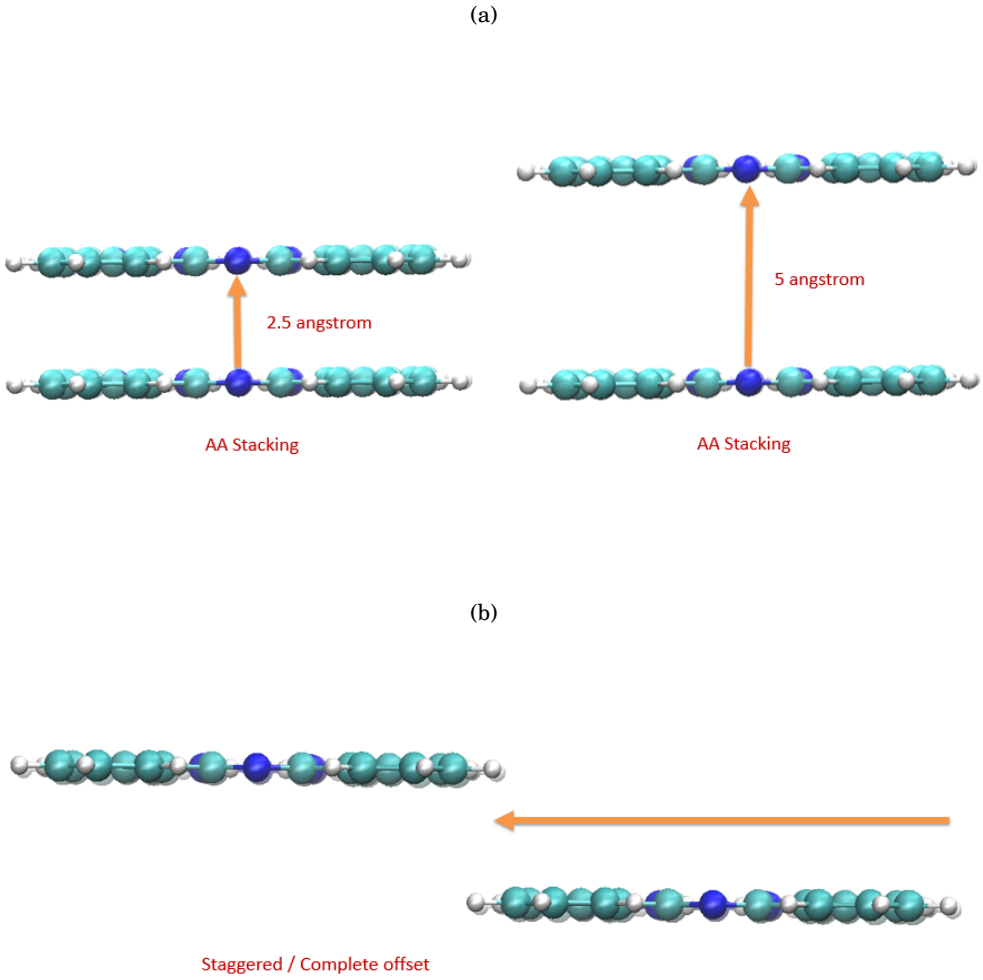

FIGURE 3.2. (a) Figure depicting phthalocyanine AA stacking for two molecules; (b) Figure depicting two phthalocyanine molecules offset from their original AA (eclipsed) stacking to a completely staggered position

3.4.2 Methodology: Radial distribution function

Radial distribution functions (RDF) can be determined both experimentally and from simulation, allowing a direct comparison. In addition, all thermodynamic quantities can be derived from an RDF under the assumption of a pair-wise additive potential energy function.[14]. We used the

(a)

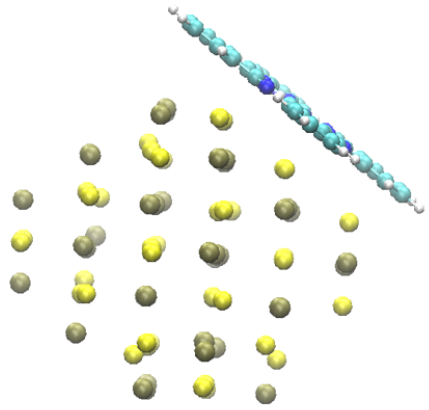

FIGURE 3.3. (a) Figure depicting a 1.5 nm PbSe nanocrystal with a single phthalocyanine molecule on one of the {111}Pb-terminated facets

radial distribution function, $g(r)$, which gives the probability of finding a particle at a distance r from another particle. If we count the appearance of two molecules at separation r, from $r = 0$ to $r = \infty$, we can get the radial distribution function, $g(r)$. The radial distribution function is a useful tool to describe the structure of a system as a function of radial distance. Consider a spherical shell of thickness δr at a distance r from a chosen atom. The volume of that shell is given by:

$$V = \frac{4}{3}\pi(r+\delta r)^3 - \frac{4}{3}\pi r^3 \approx 4\pi r^2 \delta r. \tag{3.6}$$

If the number of particles per unit volume is ρ, then the total number in the shell is $4\pi\rho r^2\delta r$, and the number of atoms in the volume element varies as r^2.

Radial distribution functions can be measured experimentally using X-ray diffraction [8]. To calculate the pair distribution function from a simulation, the neighbors around each atom or molecule are sorted into distance bins. The number of neighbors in each bin is averaged over the entire simulation. For example, a count is made of the number of neighbors between 2.5 and 2.75 angstroms, 2.75 and 3.0 angstroms, and so on, for every atom or molecule in the simulation.

The radial distribution function for molecules is usually measured between two fixed points, such as between the centers of mass. Radial distribution functions calculated from systems of several hundred thousand to one million atoms have been useful in studies of long-range order in self-assembled alkanethiol monolayers [14]. In this thesis, to describe phthalocyanine - phthalocyanine interactions and phthalocyanine - nanocrystal interactions, computing radial distribution functions between the centers of mass of pairs of molecules gives us a statistical description of the local structure of the molecules in the simulated system.

3.4.3 Methodology: Isolated phthalocyanine study

Having optimized the LJ parameters against *ab initio* data to model the forces between phthalocyanine molecules in the previous section, we can now begin to simulate and study systems involving phthalocyanine molecules in the absence and presence of PbSe NCs. We begin by studying a system of isolated phthalocyanine molecules in the absence of a NC, as shown in Figure 3.4. The system was thermalized at 300 K using a Nosé-Hoover thermostat [26] for a period of 1850 ps using a time step of 1 fs. Deibel *et al.* [4] reported that a β-form density of phthalocyanine exists in a liquid crystalline phase. We study the radial distribution function of the centers of mass of the phthalocyanine molecules to validate what we do, indeed, observe a liquid crystalline phase of phthalocyanine at a temperature of 300 K. The main purpose of this study was to understand how phthalocyanine molecules behave in an isolated system, which will be discussed in the results section of this chapter.

3.4.4 Methodology: Isolated single nanocrystal study

Having acquired a baseline configuration of phthalocyanine molecules in the absence of a PbSe NC, we then studied a system containing a single, isolated, NC in a box filled with phthalocyanine molecules.

We performed MD runs using two different arrangements of phthalocyanine molecules. In the first arrangement, we covered the single NC with layers of phthalocyanine molecules on all facets of the 4 nm diameter NC. Figure 3.5 shows 90 phthalocyanine molecules covering all facets, with an equal number of molecules per unit area available on each facet: {111} Pb-rich,{100} Se-rich,

(a)

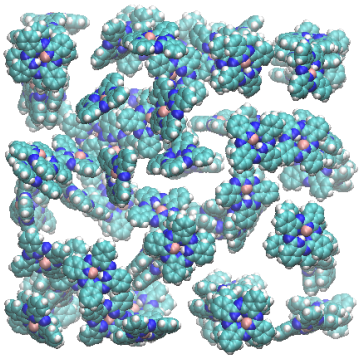

FIGURE 3.4. (a) Figure depicting initial configuration of a system of phthalocyanine molecules

and {100} PbSe alternating facets. In the second system of isolated nanocrystal study, we took a very large 10 nm diameter cubic simulation box filled with a single nanocrystal packed with 2000 phthalocyanine molecules at a β-form density, as discussed in section 1.3.1.

(a)

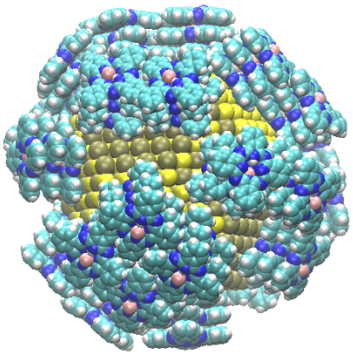

FIGURE 3.5. (a) Figure depicting the original arrangement of phthalocyanine molecules adsorbed onto different facets of nanocrystal in AA stacks.

The system was thermalized at 300 K using a Nosé-Hoover thermostat [26] for a period of 1850 ps using a time step of 1 fs. The nanocrystal was considered as a rigid body, fixed in space, throughout the simulation time. The rigid-body algorithm used by LAMMPS, rigid/nvt, was described in the paper by Kamberaj [12]. LAMMPS has a rigid/nvt style that performs a constant-volume, constant-temperature NVT integration using a Nosé/Hoover thermostat. It was necessary to simulate for a sufficiently long time (here, nearly 2 ns) to minimize fluctuations in the temperature and energy of the system. The temperature and energy of the system was observed to achieve an acceptable standard deviation of less than 1% of the mean value after around 2 ns of simulation.

The main purpose of this study was to determine the interations of the phthalocyanine molecules in the presence of a single NC. Once the system was considered to be adequately thermalized, after 2 ns, estimates of the radial distribution functions of the phthalocyanine molecules around the nanocrystal were determined as described in the previous section. This procedure repeated the simulation procedure adopted earlier for a box filled with a high density of phthalocyanine molecules.

3.4.5 Methodology : Two nanocrystal study

A system involving two nanocrystals in relatively close proximity to one another and in the presence of the phthalocyanine molecules was then studied. This system was equilibrated in the same manner described above. In order to study the interaction between nanocrystals, we allowed the NCs to translate and rotate freely as a rigid body. The two nanocrystals were initially arranged face to face and placed 30 angstroms apart (a NC center-to-NC center distance of 71 angstroms); see Figure 3.6. In this way, the whole system (NCs and phthalocyanine molecules) were maintained at thermal “equilibrium” over the entire course of the simulation, where fluctuations in the energy were assumed to be small enough that the system achieved at least a locally steady-state condition. This study was undertaken in order to investigate how phthalocyanine molecules behave in the presence of two NCs (foreshadowing the NC superlattice calculations) and how nanocrystals interact with each other in the presence of phthalocyanine molecules.

(a)

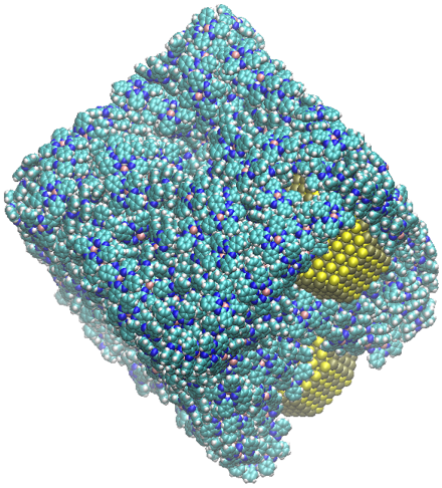

FIGURE 3.6. (a) Figure depicting isolated two nanocrystal system in presence of phthalocyanine molecules

3.4.6 Methodology : Nanocrystals in a BCC superlattice

In a final test case, a system involving NCs arranged in a periodic BCC superlattice was studied. The purpose of this study was to investigate the interaction between NCs that are constrained by the geometry of a superlattice by imposing periodic boundary conditions in all three Cartesian directions; see Figure 3.7.

3.5 Results and discussion

3.5.1 Results: Binding Energy study

As an accurate baseline against which to measure the results of the semi-empirical models of larger systems, we first calculated the binding energy of a system containing a PbSe NC with a single phthalocyanine molecule placed on different facets of the NC surface, as mentioned in the simulation methodology section above. We considered a much smaller NC, 1.5 nm in diameter, *i.e.,* $Pb_{40}Se_{40}$, due to limitations imposed by the computational expense of the *ab initio* DFT calculations. The DFT-derived binding energies we found are listed in Table 3.1. This DFT study

(a)

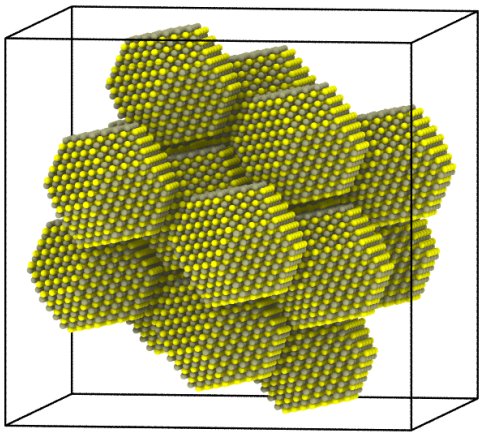

FIGURE 3.7. Figure depicting NCs arranged in a BCC periodic lattice

Nanocrystal facet	Binding energy (in eV)
100 facet (alternating Pb, Se)	-0.42
111 Se terminated facet	-0.22
111 Pb terminated facet	-0.43

TABLE 3.1. Table listing the the DFT-derived binding energies of a phthalocyanine molecule with different surface facets of a PbSe NC

clearly suggests that the phthalocyanine molecules prefers to bind to the Pb-rich {111} facet of the NC versus an Se-rich {111} facet, by a factor of roughly 2:1. However, it also shows the the mixed Pb-Se {100} facet is competitive with the Pb-rich {111} facet, having almost an identical binding energy. Thus, the DFT binding energies suggest that we can expect to see phthalocyanine molecules adsorbed to both the Pb-terminated {111} facet and the {100} facet in roughly equal amounts, with lower tendency to bind to Se-terminated facets.

3.5.2 Results: Force Field Validation

As described in the methodology section above, we conducted three trials to help fit the LJ parameters to DFT-derived data. In the first test, a system of two phthalocyanine molecules were placed at a distance of 2.5 angstroms apart in an eclipsed AA stacking as shown in Figure 3.2a. The second phthalocyanine molecule was then moved vertically from the surface of the first molecule, increasing their separation in steps of 0.1 angstroms, as shown in Figure 3.2a. Results are shown in Figure 3.8 for the energy as a function of this separation distance modeled both using (i) an accurate DFT study employing **Gaussian** with a dispersion-corrected B3LYP-D3 functional, as discussed in section 2.2.4, and (ii) a classical energy minimization using the OPLS force field described in section 3.3. The interaction energy was calculated as a function of distance between the two phthalocyanine molecules adopting an AA-stacking. The LJ parameters were then optimized to fit the DFT curve. The resulting optimized Lennard-Jones parameters (shown as an inset to Figure 3.8) and the resulting interaction energy curves can be seen in Figure 3.8. As can be seen in Figure 3.7, a minimum interaction energy of about -40 kcal/mol was achieved when the two phthalocyanine molecules were placed 3.6 angstroms apart. This minimum energy distance is in agreement with that found for the β-form phthalocyanine - phthalocyanine distance, which showed the equilibrium distance to be 3.6 angstroms [17].

In the second test, a system of two phthalocyanine molecules was moved laterally in steps of 0.1 angstroms from an initial AA stacking to a completely staggered position calculating the energies using both DFT and a semi-empirical model study. As can be seen from the interaction energy curve in Figure 3.9, the minimum interaction energy using DFT was found for a structure in which the two phthalocyanine molecules were offset by 1.2 angstroms, compared to the offset of 1.5 angstroms obtained using a semi-empirical approach. These results are close to results for the β polymorph of phthalocyanine in which an offset of 1.64 angstrom was reported by Robertson *et al.* [9, 17] using X-ray diffraction studies. Given that the β polymorph is not exactly the same configuration as in the test configuration here, the close comparison between experimental studies [9, 17] and simulation validates the force field we used for the following phthalocyanine studies.

The third study involved a system in which a single phthalocyanine molecule was placed on a {111} Pb-rich facet of a PbSe NC. We considered a 1.5 nm diameter nanocrystal, $Pb_{40}Se_{40}$, as

(a)

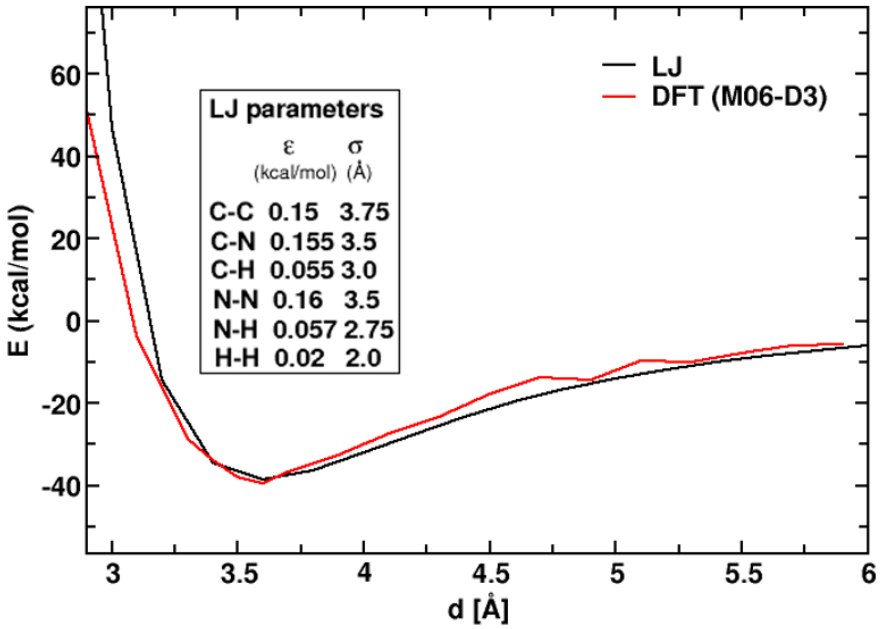

FIGURE 3.8. (a) Figure depicting the interaction energies of two AA stacked phthalocyanine molecules as a function of separation distance. The optimized LJ parameters that give rise to the semi-empirical curve are provided as an inset.

shown in Figure 3.10 due to practical limitations in using an *ab initio* DFT study. To validate the force field that describes the interaction between the phthalocyanine molecule and the surface of the PbSe NC, we used the LJ parameters for Pb and Se taken from the data provided by Kaushik *et al.* [37] and calculated the interaction energy between the PbSe NC surface and a phthalocyanine molecule as we increasingly separated the distance between the phthalocyanine molecule and a {111} Pb-terminated NC facet. See Figure 3.9. Comparison of both the DFT curve and Lennard-Jones curve shows that there is an offset of approximately 0.25 angstrom and an interaction energy difference of less than 5 kcal/mol. This shows that there is a good correlation between the results from the DFT and the semi-empirical intermolecular potential models.

(a)

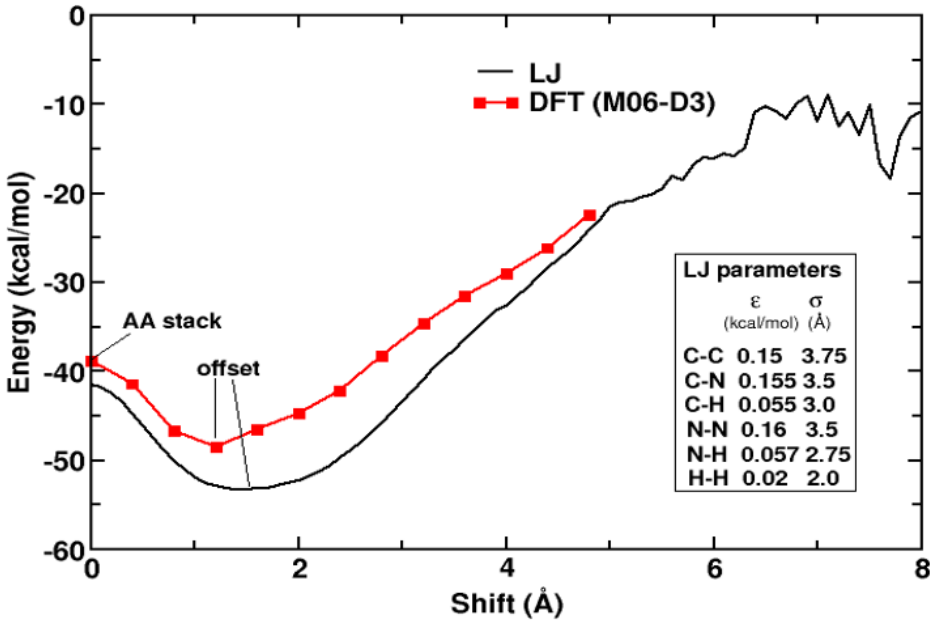

FIGURE 3.9. (a) Figure depicting the interaction energy as a function of offset distance between two phthalocyanine molecules. Optimized values for the LJ parameters are shown in the inset.

3.5.3 Results : Isolated nanocrystal study

We started our study of nanocrystals in a matrix of phthalocyanine molecules by simulating a single, isolated, 4 nm diameter, truncated octahedral NC surrounded by a limited number of phthalocyanine molecules in order to establish a 'baseline' observation of the adsorption behavior of phthalocyanine molecules around a surface of a single NC, as described in sections 3.2. and 3.4.

For this MD study, the NC was constrained as a rigid body held fixed in space (with the atoms unable to move) and the surrounding phthalocyanine(Pc) molecules were equilibrated at a temperature of 300 K for a period of 3 ns. In the first system, NC facets were covered with AA-stacked layers of phthalocyanine ligands, as described in figure 3.4 and allowed to equilibrate as described earlier. The phthalocyanine molecules were initially placed on different facets. The interlayer offset was 4 angstroms between layer 1 and 2 and around 4 angstroms between layer 2

(a)

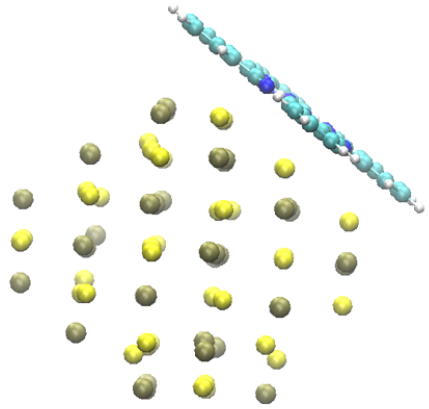

(b)

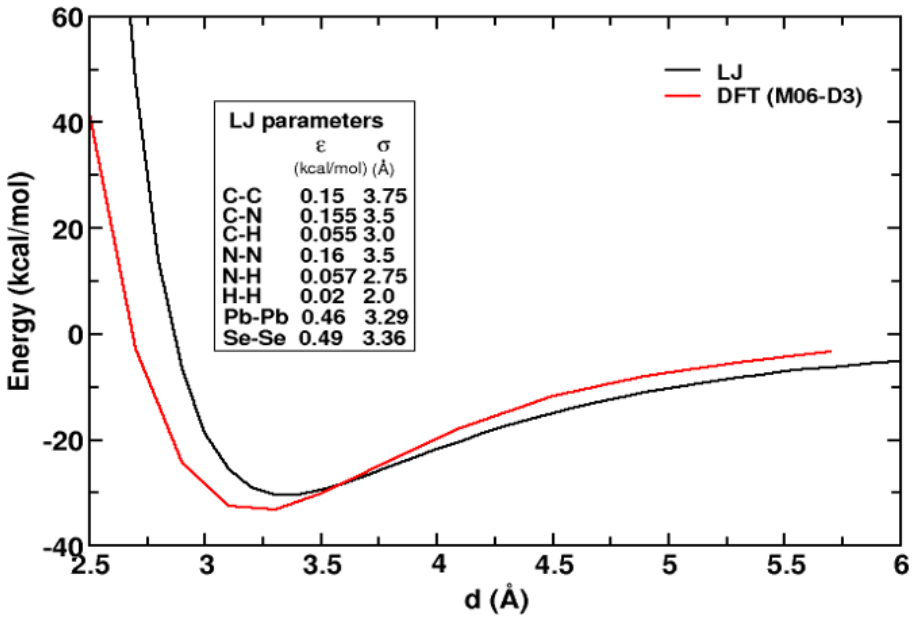

FIGURE 3.10. (a) Figure depicting a 1.5 nm diameter PbSe nanocrystal with a single phthalocyanine molecule on one of the {111}Pb-terminated facets (b) Plot depicting the interaction energy as a function of separation distance between the phthalocyanine molecule and a {111} Pb-terminated facet

and 3. The phthalocyanine molecules were initially placed at a lateral distance of 20 angstrom center of mass (COM - COM) distance from each other.

The phthalocyanine molecules of Pb-terminated facets tended to stay adsorbed to the surface of NC and the phthalocyanine molecules on the Se-terminated facets largely maintained an AA stacking with an offset of 1.6 angstroms, close to the optimum offset calculated for isolated phthalocyanine - phthalocyanine interactions. The peak **a,b** in the pair distribution function indicate the closest distance between phthalocyanine COMs in layers 1 and 2. The peaks **d,e** indicate the distance between phthalocynaine COMs in layers 1 and 3. The peak **f** shows the lateral distance between COMs at 13 angstroms, which indicates that the phthalocyanine molecules are aggregating laterally. Figure 3.9a shows the radial distribution of the centers of mass (COM) of phthalocyanine molecules. We calculate the displacement vectors of the COMs relative to the initial configuration of the simulated system by subtracting the COM of the position of each phthalocyanine in the current configuration from the particle's position in the initial configuration. Figure 3.11b shows a color-coded visualization of the magnitude of COM displacements that we observed. We noted that the inner layers of stacked phthalocyanine molecules moved laterally to be close to the other layers, indicating a preference to maximise interactions with both the NC and its phthalocyanine neighbors.

Further analysis of this system containing an isolated NC with a few layers of phthalocyanine molecules was subsequently revisited with a more densely packed phthalocyanine system. For this study we used a simulation box of length 10 nm cubed and filled with 300 phthalocyanine molecules and a single PbSe nanocrystal, as shown in Figure 3.12a. The PbSe nanocrystal was treated as a rigid body, held fixed as discussed earlier, and the phthalocyanine molecules were equilibrated around it at a temperature of 300 K for a period of 2 ns. The temperature and energy of the system was observed to achieve a relatively constant mean value with an acceptable standard deviation of less than 1% of the mean value of the energy. We consider phthalocyanine molecules bounded (adsorbed) on the NC surface, if these phthalocyanine molecules are less than 5 angstroms from the surface of the NC. Out of the 1000 phthalocyanine molecules, we find that approximately one-third (around 110) of the Pc molecules are adsorbed on the NC surface. We observe that the remaining phthalocyanine molecules which are considered to be non-bounded

(a)

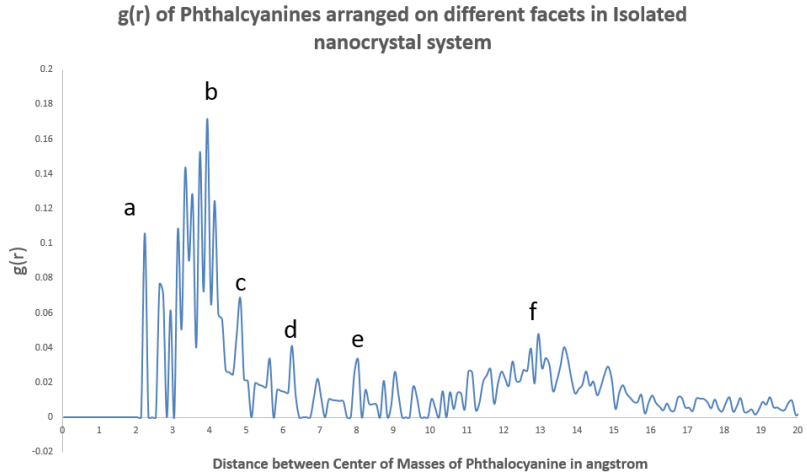

(b)

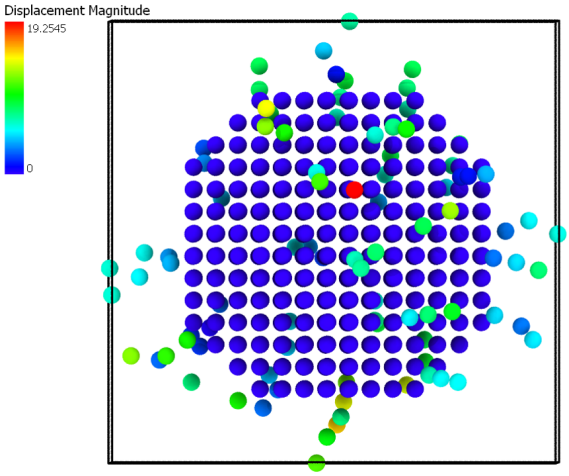

FIGURE 3.11. (a) Figure depicting the radial distribution function of the centers of mass of phthalocyanine molecules; (b) Color-coded visualisation of the magnitude of phthalocyanine displacements from their original positions.

molecules have a pronounced tendency to be bounded to one another. Figure 3.13 shows the pair distribution of COM of phthalocyanine molecules in this arrangement.

(a)

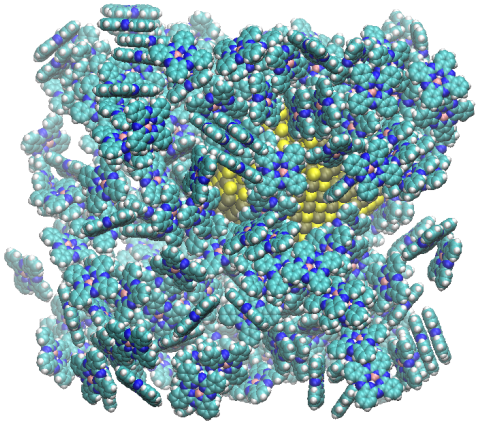

(b)

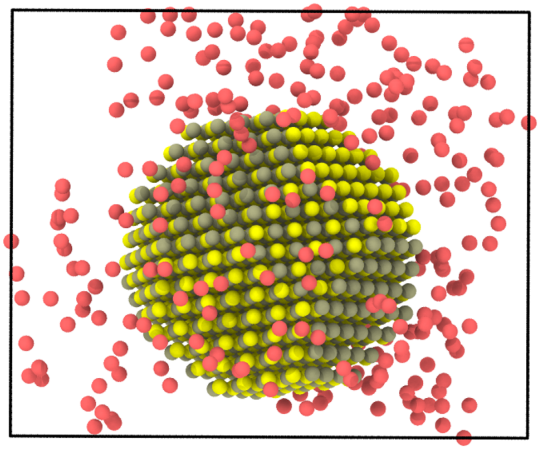

FIGURE 3.12. (a) Figure depicting the final snapshot of an MD simulation of a phthalocyanine-covered PbSe nanocrystal at 300 K; (b) Thermalized MD snapshot showing the centers of mass of phthalocyanine molecules around the nanocrystal.

Figure 3.12b shows the interaction of thermalised, quasi-equilibrated phthalocyanine molecules in the presence of the nanocrystal.A quantitative analysis of the fraction of phthalocyanines

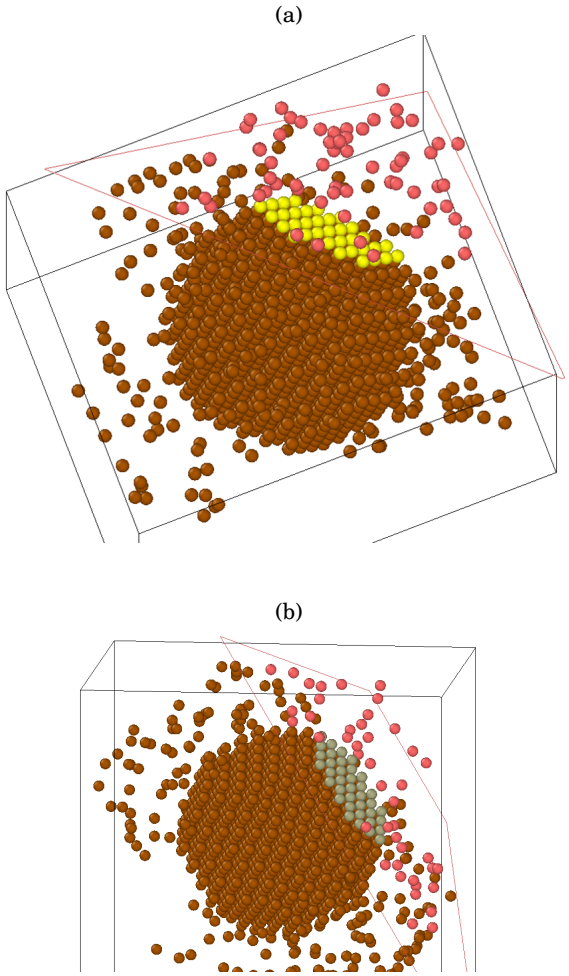

FIGURE 3.13. (a) Figure depicting the approach used to identify the molecules in "slices" in the area above the surface of a {111} Pb-terminated facet (shown in yellow) of the PbSe NC for post-processing; (b) Similar depiction for "slicing" above a {111} Se-terminated facet (shown in green) of the NC. In both the cases, the Pc molecules on the respective facet is colored in red.

(a)

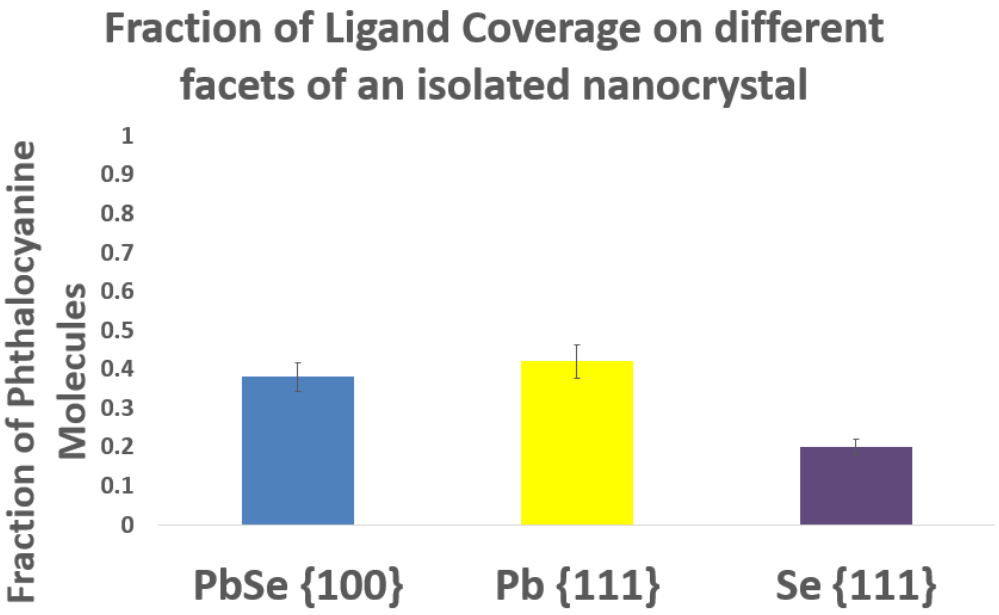

FIGURE 3.14. (a) Plot depicting the fraction of phthalocyanine molecules on different facets of a truncated PbSe nanocrystal with the {111} Pb-rich facet (yellow bar), the {111} Se-rich (purple bar) facet and the {100} Pb-Se alternating facet (blue bar). The relative distribution of the three fractions matches well with the results of the DFT-derived binding energies, in that mixed Pb-Se {100} and Pb-terminated {111} fractions are similar in magnitude, while the fraction on Se-terminated {111} is roughly only half the amount of the other two.

preferring to adopt {111} Pb-terminated,{111} Se-terminated and {100} alternating Pb- and Se-terminated facets was achieved by observing the nature of "slices" of the system in the region above the surface of the NC for different facets and calculating the number of phthalocyanine molecules on each facet using **OVITO**, as described in section 2.2.6 and shown in Figure 3.14. After “slicing” the nanocrystal for analyzing the disposition of phthalocyanine on different facets, we calculated the fraction of phthalocyanines on a given facet. After calculating the number of phthalocyanine molecules on different facets, we observed, from Figure 3.14, that the majority of phthalocyanines prefer to adsorb onto the {111} Pb-terminated facet, which is supported by the binding energy study discussed in section 3.5.1.

This study gave us both a qualitative and a quantitative picture of the behaviour of phthalocyanine molecules in presence of NC. However, there might be different types of interactions between two or more NCs, which will be described in the remaining sections.

3.5.4 Studies of a pair of NCs and in a superlattice in a box of phthalocyanine molecules

Before discussing a study of NCs in a superlattice, we study a pair of isolated "two nanocrystals" in a system filled with phthalocyanine molecules. For this study, both of the rigid NCs were free to rotate and translate in the system (refer to section 3.4 for the simulation methodology). The whole system was equilibrated using an NVT ensemble MD simulation held at a constant temperature of 300 K for a period of 1 ns. The energy and temperature of the system was allowed to come to a quasi-steady-state, as discussed in earlier sections.

The NCs were initially placed at a distance apart of 55 angstroms in terms of their NC center-to-NC center distance, which is equivalent to a distance of 15 angstroms apart for the outer surfaces of the NCs. Figure 3.15 shows the final configuration of the system where it can be seen that the phthalocyanine molecules stay in-between the nanocrystals. After equilibration for further 2 ns, the NC center-to-NC center distance was found to have decreased only very slightly, to 54.2 angstroms, which suggests only very limited influence of one nanocrystal on another. Even after equilibrating the system for another 2 ns, it was found that the NC-NC center-to-center distance remained essentially the same (54.2 angstroms). This clearly indicates

that the interaction of one NC is almost unfettered by the presence of the other NC in the system. This study of an isolated "two" nanocrystal acts a precursor to the superlattice study,because in a superlattice study, pairs of nanocrystals are translationally and rotationally constrained because of the presence of other nanocrystals nearby.

(a)

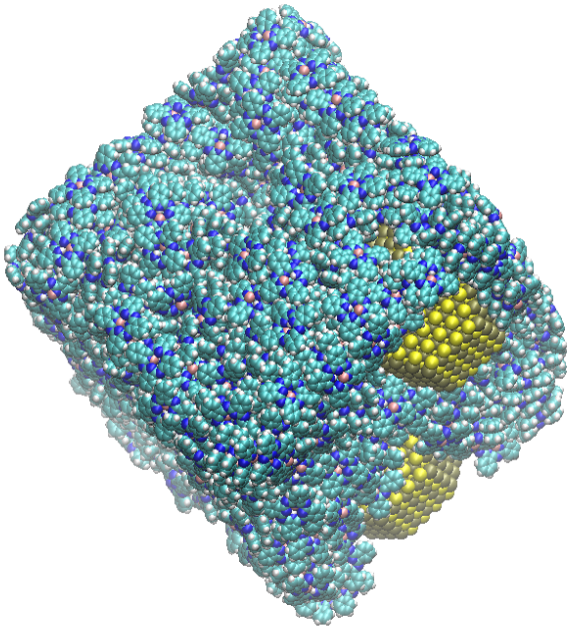

FIGURE 3.15. MD snapshot after 2 ns of simulation of two isolated nanocrystals in the presence of phthalocyanine molecules

Finally, we examined the interaction between pairs of NCs within a periodic BCC superlattice of NCs by imposing periodic boundary conditions on the system. As discussed in an earlier section, 1.1.3, the BCC superlattice was found to be the most energetically stable superlattice for PbSe NCs [61].

We have considered two systems containing 16 nanocrystals in a BCC arrangement, with varying density of phthalocyanines; one box containing 1000 and the second box containing 2000 phthalocyanine molecules. The distance between nearest neighbors was initially well beyond the cut-off used for van der Waals interactions. The atoms within the NCs were held rigid, but the rigid body of the NC was free to translate and rotate, as described for the preceding system. The

system was again thermalized at a temperature of 300 K in an NVT ensemble MD simulation employing a 1 fs time step, with the time evolution followed for about 2 ns. Figure 3.16 shows the inter-NC center-to-center distances for the two different densities of phthalocyanine molecules. The first two peaks $a_1 and a_2$ corresponding to the 1000-molecule system indicate the nearest NC-NC center distance and the peaks b_1, b_2, b_3 of the 1500-molecule systems correspond to the nearest center-center distance of two NCs in BCC superlattice. We calculated the edge-edge distance in both these systems, by approximating the NC as a sphere and taking the difference between the center-to-center distance and the diameter of the NC. The mean edge-to-edge : NC-NC distance was found to be 7 angstroms and 13 angstroms corresponding to the two systems, respectively.

(a)

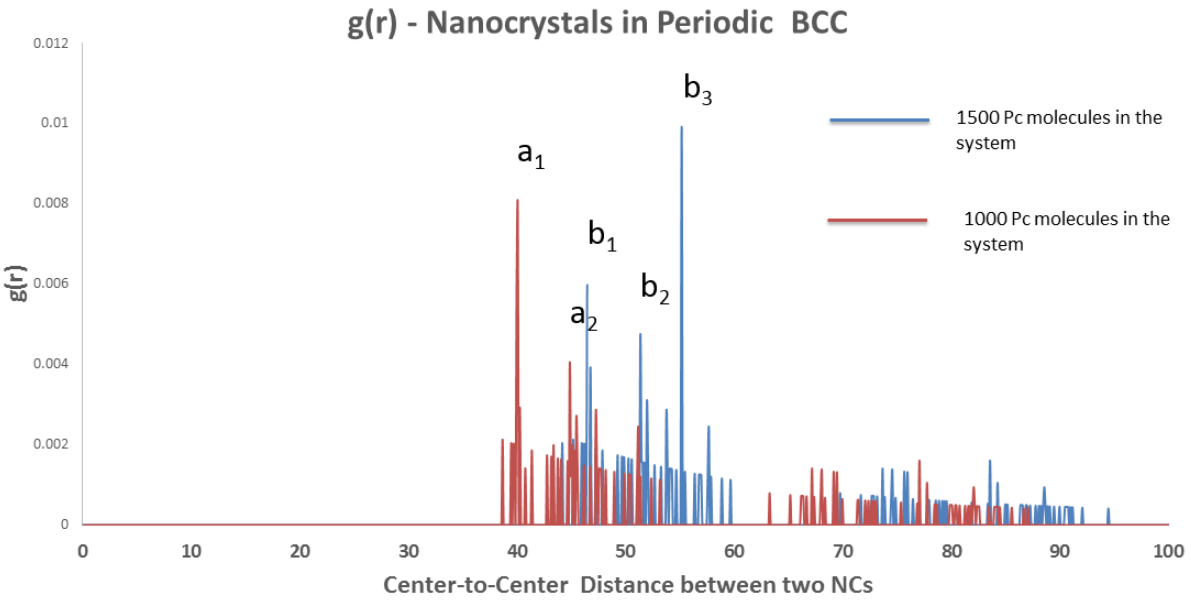

FIGURE 3.16. Plot of radial distribution as a function of center-to-center distance of NCs in BCC periodic superlattice with different densities of phthalocyanine molecules in the system

We will now compare the NC-NC distance of our system with experimentally used systems

Study	Spacer	Reference	Mean Edge-Edge NC distance
Expt.	Oleic acid ligand	Quan *et al.* [61]	36 angstrom
Expt.	Oleic acid ligand	Schapotschinikow *et al.* [33]	28 angstrom
Expt.	1-3-hexene-di-thiol	Luther *et al.* [28]	21 angstrom
Comp.	Oleic acid ligands	Kaushik *et al.* [37]	30 angstrom
Comp.	Metal-free phthalocyanine	this work	10 angstrom

TABLE 3.2. Table listing the edge-to-edge NC distances in a periodic BCC lattice using different ligands as reported in the literature, and compared to the edge-to-edge NC distance reported in this study using phthalocyanine molecules as spacers. *Note: Expt. represents experimental work and Comp. represents computational work*

involving long alkyl chains [33, 61] and thiol-based ligands [28].

Table 3.2 shows the edge-edge NC-NC distances of PbSe NCs in BCC superlattices reported experimentally compared to the mean edge-edge NC-NC distances found here for the phthalocyanine molecules. We can conclude that NC-NC distance in the presence of phthalocyanine is the lowest amon all other reported ligands mentioned earlier.

For effective charge transfer to occur, the nearest neighbor distance in self-assembled NC should be less than 1 nm [37]. Based on these results, we can say that the inter-NC distance of nanocrystals arranged in a BCC lattice in the presence of phthalocyanine spacer molecules is substantially reduced and suggests that this is a promising approach to investigate experimentally. However, due to constraints in computational time, as discussed earlier, with the explicit all-atom model and an extremely large system of 140,000 atoms, this study cannot totally rule out NC aggregation given sufficient time. We will discuss in the next chapter the limitations of the all-atom model used here and recommend the use of coarse-grained representations to improve computational efficiency of a NC superlattice-phthalocyanine system. It is also clear that Molecular Dynamics may not, ultimately, be the best approach given the tendency of the spacer molecules to aggregate. In hindsight, a Monte Carlo or Replica Exchange MD approach are perhaps more likely to give results closer to the true equilibrium condition. Nevertheless, this

is a promising feasibility study that warrants further investigation.

CHAPTER 4

CONCLUSIONS AND FUTURE PROSPECTS

4.1 Conclusions

4.1.1 General remarks on colloidal quantum dots

In the last quarter century, the field of colloidal quantum dots has advanced from pioneering chemical synthesis, to physical characterization studies, to improvements in materials processing, and to the development of electronic devices. All of these developments have led to promising and improving device performance through novel architectures. The combination of tunable band gaps with straightforward solution-processed fabrication involving self-assembly gives colloidal quantum dots considerable potential for low-cost and effective optoelectronic applications. Progress in the field has advanced from early studies of protocols for colloidal NC synthesis to creation of NCs with tunable optoelectronic properties and self-assembly into functional superstructures. Although an immense number of publications (approximately 14,000 journal articles) [**?**] exist on colloidal quantum dots, our understanding of the underlying physics and chemistry of building quantum dot arrays continues to grow and every major breakthrough paves the way for novel applications of quantum dots. [36],[29],[30],[32]. Some of the open questions related to quantum dot technology involve (i) the nature of the NC surface (ii) spacer design (iii) influence of spacer chemistry and surface faceting on the coupling between NCs.

In summary, in this thesis, we have investigated one of these open challenges, studying the viability of a new class of planar, charge-conducting spacers in advance of experimental study.

4.1.2 Behavior of planar, charge-conducting spacers in nanocrystals

We have presented an explicit all-atom representation of phthalocyanine "capped" nanocrystals of experimentally relevant size (4 nm) in vacuum. We have determined force fields that we have shown reasonably describe the interaction between these planar ligands and nanocrystals, by comparison to *ab initio* calculations. We studied three test cases of increasing complexity: (1) an isolated single NC; (2) a pair of NCs within the range of their intermolecular potential and (3) a NC superlattice arranged in a BCC symmetry. In each case, the NCs are surrounded by a high density of phthalocyanine molecules. These Molecular Dynamics simulations have shown the preference of phthalocyanine molecules to adsorb on 111 Pb-rich facets on the surface of the truncated octahedral PbSe NC. We calculated the edge-to-edge distance of nanocrystals in a BCC superlattice and observed a mean edge-to-edge distance between two NCs in a BCC superlattice to be 7 angstroms and 13 angstroms with different densities of phthalocyanine molecules in the system. We also showed that the preferred edge-to-edge distance between nanocrystals is reduced by 11 angstroms compared to thiol-based ligands [28] and about 20 angstroms compared to typical ligands composed of long alkyl chains [37]. This is a considerable advantage in terms of charge transport.

The behavior of phthalocyanine-capped NCs was determined using an explicit all-atom model. This "baseline" study which serves as a reference for using this class of planar-charge conducting molecules in the self-assembly of colloidal nanocrystals. In this study, we considered phthalocyanine due to their semiconducting nature which arises from their electron delocalization. As described in chapter 1, section 1.3.1, the phthalocyanine ring offers the possibility of incorporating about 70 different metal atoms,which makes the metallo-derivatives of phthalocyanine, an interesting class of ligands for nanocrystal self-assembly.

Due to the large size of these NC superlattice systems, an all-atom description for the NC capping layer of phthalocyanine molecules and realistically sized NCs would be computationally too expensive to consider. In order to save computational time, coarse-grained methods can be

applied. Hence, the obvious next steps are to move towards coarse-grained systems, which will be discussed in the next section.

4.2 Future Prospects

4.2.1 Metallo-derivatives of phthalocyanines as spacers in NC self-assembly

The class of planar charge-conducting molecules encompassing phthalocyanines and their metallo-derivatives offer considerable potential for their use as ligands in nanocrystal self-assembly. Phthalocyanine and its metallo-derivatives have been studied as targets for low band gap molecular solar cells, photosensitizers, *etc.*, as described in section 1.3.1. Metallo-derivatives of phthalocyanines have been recently used as organic photovoltaic cells. [23],[34], [35], [31], [47]. An impressive solar efficiency of around 5.5% was obtained using a thin film solar cell made of (CuPC)/C_{60} [44], [2]. Recently, the use of butyl-substituted zinc phthalocyanine in dye-sensitized solar cells was reported by Cid *et al.* [40] who found that these substituted zinc phthalocyanines not only avoided the formation of molecular aggregates, but arranged the excited states to permit charge transfer, achieving efficiencies above 3% [53]. Titanyl phthalocyanine, TiOPc, in particular, has become of interest because of its semiconducting as well photoconductivity properties [13]. Law *et al.* showed that titanyl phthalocyanine of the Y-polymorph (Y-TiOPc) has the best photoconductivity among the H_2Pcs, CuPcs, VOPc, AlClPc, TiOPcs of the other polymorphs [60]. The photoconductivity and charge-transport properties of TiOPc vary substantially depending on the crystal phase it adopts in the solid state [56]. TiOPc is known to form various polymorphs that are responsible for differences in stacking modes and molecular alignment [43], [11]. While the α - triclinic phase-TiOPc is reported to be an excellent p-type semiconductor with a broad spectral absorption range suitable for use in solar cells [65].

Figure 4.1 shows the space-filled model of TiOPc and the stacking of α - TiOPc crystal showing the π - stacking structure with a concave pair and a convex pair with significant molecular overlaps and very short intermolecular distances.Figure 4.2 shows the binding energies of different stacking arrangements of TiOPc molecules with themselves and with different facets of PbSe NC.It is quite clear that the binding energy of TiOPc molecule to PbSe NC is greater than

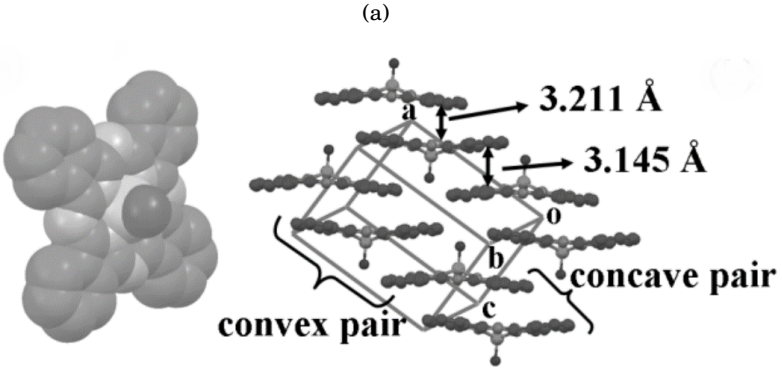

FIGURE 4.1. Space-filling molecular model of titanyl phthalocyanine, b. molecular stacking of α-TiOPc crystal showing the π-stacking; figure reproduced from [50]

TiOPc-TiOPc binding energies, which indicates that Titanyl phthalocyanine prefers binding to the NC than themselves, which indicates that there could be possibly no aggregation of these spacers in the system, making them an interesting prospect to study their behavior in NC superlattices.

4.2.2 Coarse-grained model for a phthalocyanine-capped NC superlattice

To develop a coarse-grained model which is less computationally intensive to simulate and yet still reproduces the same physical behavior as one in which all the atoms are modeled explicitly requires that considerable care needs to be taken in the following choices: (i) choosing pseudoatom sites that are designed to represent a combined group of multiple atoms depends on the number of pseudoatom sites and how they are connected to a more detailed model; (ii) defining an effective energy function U_{CG}, which defines the interactions between the pseudoatoms should be chosen so as to reproduce the same thermodynamic properties as the reference model.

Coarse-graining a system of phthalocyanine-capped nanocrystal superlattice consisting of 2000 phthalocyanine molecules in the presence of 16 4 nm-diameter PbSe NCs, given that each phthalocyanine molecule consists of 58 atoms, will require choosing pseudoatom sites with considerable care. Melis *et al.* [24] studied zinc-phthalocyanine by means of an atomistically informed coarse-grained model using classical Molecular Dynamics, where they described each ZnPc as a bead (with only two translational degrees of freedom) that interacts with the lattice

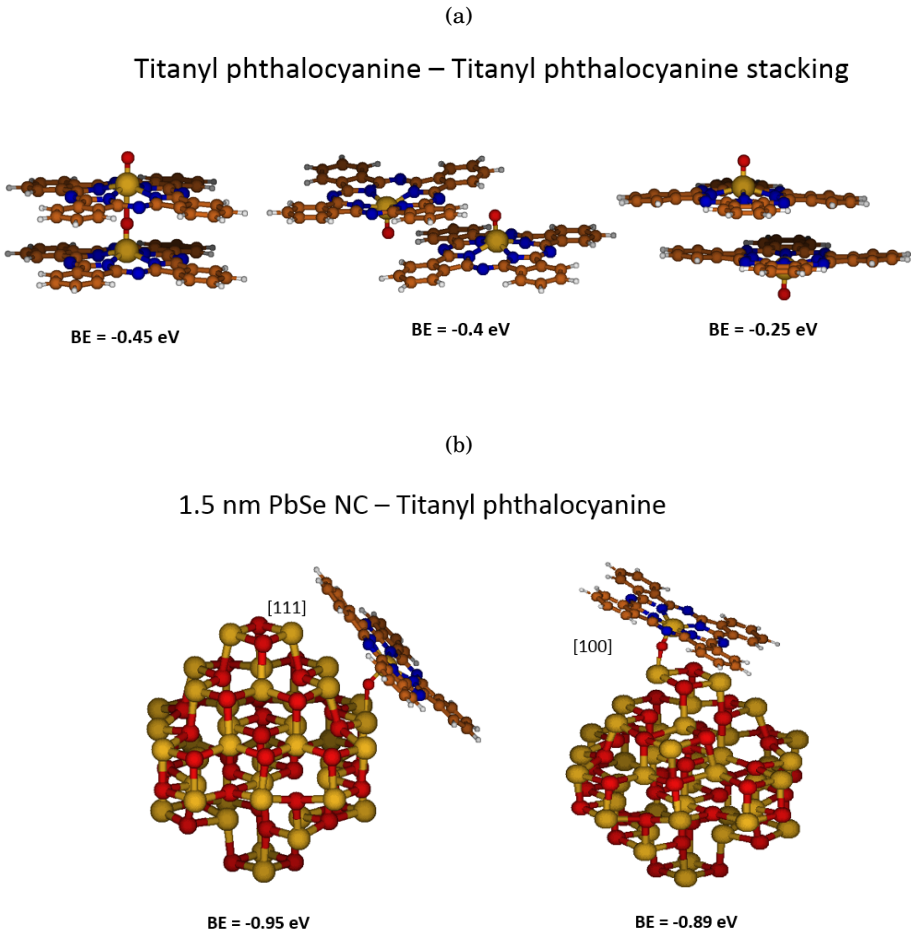

FIGURE 4.2. a. Different stacking arrangements of Titanyl phthalocyanine with respective binding energies, b. Titanyl phthalocyanine on different facets of NC with respective binding energies

and the other molecules via effective potentials. Apart from Melis *et al.*,coarse-graining of phthalocyanine molecules is an area which is still undefined in the literature.

Each phthalocyanine molecule can be represented as 6 beads, with each isoindole unit as an individual bead, amounting to 4 isoindole beads connected with N and H atoms.The coarse-grained potential for bonded interactions is a Boltzmann inversion of corresponding probability density distribution. The non-bonded potential can be found by fitting radial distribution functions for bonded interactions.An integration time step of 100 fs allows faster simulation. However, the choice of time step depends on how fast beads are moving in the simulation,determined by the strength of interactions, without crashing the simulation. In theory, coarse-grained methods could allow researchers to extend the simulated time scales of phthalocyanine-capped NC systems into the microsecond regime which bridges molecular modeling with experimental investigations, whose resolution lies in the upper millisecond and microsecond range.

BIBLIOGRAPHY

[1] M. BEARD, *Comparing multiple exciton generation in quantum dots to impact ionization in bulk semiconductors: Implications for enhancement of solar energy conversion*, Nano Letters, 72 (2010).

[2] C.LIN, *High photoelectric conversion efficiency of metal phthalocyanine/fullerene heterojunction photovoltaic device*, International Journal of Molecular Sciences, 12 (2011).

[3] D. . C.MURRAY, *Pbse nanocrystal solids for n- and p-channel thin film field-effect transistors*, Science, 310 (2005).

[4] C. DEIBEL, *Charge transport properties of a metal-free phthalocyanine discotic liquid crystal*, Organic Electronics, 7 (2006).

[5] L. M. . DINEGAR, *Theory, production and mechanism of formation of monodispersed hydrosols*, Journal of American Chemical Society, 54 (1950).

[6] P. G.-S. DONG YU, *n-type conducting cdse nanocrystal solids*, Science, 300 (2003).

[7] H. FU, *Infrared colloidal lead chalcogenide nanocrystals: Synthesis, properties, and photovoltaic applications*, The Royal Society of Chemistry, 2187 (2012).

[8] N. GINGRICH AND L.HEATON, *Structure of alkali metals in the liquid state*, The Journal of Chemical Physics, 34 (1961).

[9] R. HAMMOND, *X-form metal-free phthalocyanine: crystal structure determination using a combination of high-resolution x-ray powder diffraction and molecular modelling techniques*, Journal of Chemical Society, 2 (1966).

[10] T. HANRATH, *Colloidal nanocrystal quantum dot assemblies as artificial solids*, Journal of Vacuum Science & Technology A, 30 (2012).

[11] H.YONEHARA, *Vapor deposition of oxotitanium(iv) phthalocyanine on surface-modified substrates: Effects of organic surfaces on molecular alignment*, Langmuir, 18 (2002).

[12] C. KAMBERAJ, *Time reversible and symplectic integrators for molecular dynamics simulations of rigid molecules.*, Journal of Chemical Physics, 122 (2005).

[13] K.Y.LAW, *Organic photoconductive materials: recent trends and developments*, Chemical Reviews, 1 (1993).

[14] A. LEACH, *Molecular modelling: Principles and application.*, Prentice Hall, 2 (2001).

[15] P. LINSTEAD AND J.ROBERTSON, *The stereochemistry of metallic phthalocyanines*, Royal Society of Chemistry, (1936).

[16] S. PLIMPTON, *Fast parallel algorithms for short-range molecular dynamics*, The Journal of Computational Physics, 117 (1995).

[17] J. ROBERTSON, *Beta form metal free phthalocyanine*, Journal of Chemical Society, 1195 (1936).

[18] P. SCHAPOTSCHNIKOW, *Soft hedgehogs on coarse carpets: A molecular simulation study of capped nanocrystals interacting with self-assembled monolayers of alkylthiols on a gold (111) surface*, Journal of Physical Chemistry C, 114 (2010).

[19] H. SCOTT, *Modeling the lipid component of membranes*, Current Opinion in Structural Biology, 12 (2002).

[20] W. SHOCKLEY AND H. QUEISSER, *Detailed balance limit of efficiency of p-n junction solar cells*, Journal of Applied Physics, 32 (1961).

[21] J. SIEPMANN, *Simulating the critical behaviour of complex fluids*, Nature, 365 (1993).

[22] A. STUKOWSKI, *Visualization and analysis of atomistic simulation data with ovito‚Äìthe open visualization tool*, Modelling and Simulation in Materials Science and Engineering, 18 (2010).

[23] C. B. *et al.*, *Plastic solar cells*, Advanced Functional Materials, 11 (2001).

[24] C. M. *et al.*, *Self-assembling of zinc phthalocyanines on zno (101ÃÖ0) surface through multiple time scales*, ACS Nano, 5 (2011).

[25] D. *et al.*, *A new silicon p-n junction photocell for converting solar radiation into electrical power*, Journal of Applied Physics, 25 (1954).

[26] G. M. *et al.*, *Nóse hoover chains: The canonical ensemble via continuous dynamics*, The Journal of Chemical Physics, 97 (1992).

[27] H. *et al.*, *Detailed balance limit for solar cell efficiency*, EMRS 2008 Spring Conference Symposium K: Advanced Silicon Materials Research for Electronic and Photovoltaic Applications, 159 (2009).

[28] J. *et al.*, *Optical, and electrical properties of self-assembled films of pbse nanocrystals treated with 1,2 ethanedithiol*, ACS Nano, 2 (2008).

[29] J. E. *et al.*, *Controlled chemical doping of semiconductor nanocrystals using redox buffers*, Journal of American Chemical Society, 134 (2012).

[30] J. T. *et al.*, *Quantum junction solar cells*, Nano Letters, 12 (2012).

[31] M. G. *et al.*, *Laminated fabrication of polymeric photovoltaic diodes*, Nature, 395 (1998).

[32] M. S. *et al.*, *n-type colloidal semiconductor nanocrystals*, Nature, 407 (2000).

[33] P. *et al.*, *Molecular simulations of interacting nanocrystals*, Nano letters, 8 (2008).

[34] S. M. *et al.*, *Self-organized discotic liquid crystals for high-efficiency organic photovoltaics*, Science, 293 (2001).

[35] W. H. *et al.*, *Hybrid nanorod-polymer solar cells*, Science, 295 (2002).

[36] W. K. *et al.*, *Heavily doped n-type pbse and pbs nanocrystals using ground-state charge transfer from cobaltocene*, Scientific Reports, 3 (2004).

[37] A. K. *et al.*, *Explicit all-atom modeling of realistically sized ligand-capped nanocrystals*, The Journal of Chemical Physics, 136 (2012).

[38] B. *et al.*, *Charmm: A program for macromolecular energy, minimization, and dynamics calculations*, Journal of Computational Chemistry, 4 (2004).

[39] B. O. *et al.*, *Syntheses and photodynamic activity of pegylated cationic zn(ii)-phthalocyanines in hep2 cells*, Theranostics, 9 (2012).

[40] C. *et al.*, *Molecular cosensitization for efficient panchromaticdye-sensitized solar cells*, Angewandte Chemie International Edition, 46 (2007).

[41] C. A. *et al.*, *Photodynamic properties of amphiphilic derivatives of aluminum tetrasulfophthalocyanine.*, Photochemistry and Photobiology, 76 (2002).

[42] G. S. *et al.*, *Molden - a pre- and post-processing program for molecular and electronic structures*, Journal of Computer-Aided Molecular Design, 14 (2000).

[43] H. *et al.*, *Fabrication of various ordered films of oxotitanium(iv) phthalocyanine by vacuum deposition and their spectroscopic behavior*, Chemistry of Materials, 13 (2001).

[44] J. *et al.*, *Asymmetric tandem organic photovoltaic cells with hybrid planar-mixed molecular heterojunctions*, Applied Physics Letters, 85 (2004).

[45] J. *et al.*, *Employing end-functional polythiophene to control the morphology of nanocrystal-polymer composites in hybrid solar cells*, Journal of American Chemical Society, 126 (2004).

[46] J. *et al.*, *Photogenerated exciton dissociation in highly coupled lead salt nanocrystal assemblies*, Nano letters, 10 (2010).

[47] J. H. *et al.*, *Efficient photodiodes from interpenetrating polymer networks*, Nature, 376 (2002).

[48] J. P. *et al.*, *Gaussian 70*, Quantum Chemistry Exchange Program, 237 (1970).

[49] L. *et al.*, *Structure, dynamics, and thermodynamics of passivated gold nanocrystallites and their assemblies*, Journal of American Chemical Society, 100 (1996).

[50] L. L. *et al.*, *An ultra closely π-stacked organic semiconductorfor high performance field-effect transistors*, Advanced Materials, 278 (2007).

[51] L. M. *et al.*, *Packmol : A package for building initial configurations for molecular dynamics simulations*, Journal of Computational Chemistry, 30 (2009).

[52] M. *et al.*, *Synthesis and characterization of monodisperse nanocrystals and close-packed nanocrystal assemblies*, Annual Reviews of Materials Science, 30 (2000).

[53] M. *et al.*, *Porphyrins and phthalocyanines in solar photovoltaic cells*, Journal of Porphyrins and Phthalocyanines, 14 (2010).

[54] M. S. *et al.*, *Pbse nanocrystal shape development: oriented attachment at mild conditionsand microwave assisted growth of nanocubes*, CrystEngComm, 13 (2010).

[55] N. A. *et al.*, *Molecular mechanics. the mm3 force field for hydrocarbons. 1*, Journal of American Chemical Society, 111 (1989).

[56] R. *et al.*, *Effects of thermal annealing on structure, morphology and optoelectronic properties of tiopcultrathin films*, Journal of Physics, 358 (2012).

[57] W. H. *et al.*, *Vmd : Visual molecular dynamics*, The Journal of Molecular Graphics, 14 (1996).

[58] W. J. *et al.*, *Optimized intermolecular potential functions for liquid hydrocarbons*, Journal of American Chemical Society, 106 (1984).

[59] W. P. *et al.*, *An optimized united atom model for simulations of polymethylene melts*, Journal of Chemical Physics, 103 (1995).

[60] Z. P. *et al.*, *Study of carrier generation in titanyl phthalocyanine (tiopc) by electric-field-induced quenching of integrated and time-resolved fluorescence*, Journal of Physical Chemistry B, 102 (1998).

[61] Z. Q. *et al.*, *Energy landscape of self-assembled superlattices of pbse nanocrystals*, Proceedings of the National Academy of Sciences of the United States of America, 111 (2014).

[62] S. TOXVAERD., *Equation of state of alkanes 2*, Journal of Chemical Physics, 107 (1997).

[63] J. WERNER AND H. QUEISSER, *Novel optimization principles and efficiency limits for semiconductor solar cells*, Physical Review Letters, 72 (1994).

[64] A. YANG AND C. WENG, *Structural and dynamic properties of water near monolayer-protected gold clusters with various alkanethiol tail groups*, The Journal of Physical Chemistry C, 114 (2010).

[65] H. YONEHARA AND C. PAC, *Photoelectrical properties of double-layer organic solar cells using c60 and phthalocyanines*, Thin Solid Films, 278 (1996).

[66] Y. ZHAO AND D. TRUHAR, *The m06 suite of density functionals for main group thermochemistry, thermochemical kinetics, noncovalent interactions, excited states, and transition elements: two new functionals and systematic testing of four m06-class functionals and 12 other functionals*, Theorticial Chemistry Accounts, 120 (2008).